International Journal of Civil Engineering (2023) 21:1509–1536
https://doi.org/10.1007/s40999-023-00840-6

RESEARCH PAPER

Analysis of Coupled Site and Soil–Structure Interaction Effects on the Seismic Response of Multistory Buildings According to EC-8 and ASCE7-16 Code Provisions

Mohamed Beneldjouzi[1] · Mohamed Hadid[2] · Nasser Laouami[3] · Mustapha Remki[3]

Received: 2 November 2022 / Revised: 23 February 2023 / Accepted: 15 April 2023 / Published online: 31 May 2023

Abstract

In strong seismicity areas, the structures experience seismic excitations that are affected by earthquake source effects and their propagating path, local site effects, and soil–structure interaction effects (SSIE). This study explores the impact of SSIE associated with site effects (SE) on the seismic response of multi-story buildings through a frequency domain solution within the EC-8 and ASCE7-16 code provisions. Low-to-mid-rise multistoried buildings are selected via their slenderness ratio to form systems associated with a wide range of soil profiles simulated using the random field theory. Shaking intensity ranging from moderate to strong is considered through an appropriate range of seismic magnitudes and shows that when the superstructure interacts with the nearby subsoil layers, the ground shaking level either amplifies or reduces the structural responses depending on the site category and the structure's slenderness ratio. Results indicate that, in contrast to most common SSI investigations, seismic magnitude connected with the local geology affects the response of the structure and, in certain situations, makes SSIE unfavorable. The study's findings are presented in such a way that ratios can be utilized to show how SSIE differ from SE in terms of their impact on seismic base shear (BS) and roof displacement.

Keywords Site effects · SSI · EC-8 · ASCE7-16 · Transfer function · Multistory buildings

Abbreviations

1-D	One-dimensional
1-DOF	One degree of freedom
BS	Base shear
DTF	Displacement transfer function
FB	Fixed base
GMPE	Ground motion prediction equation
K&T	Kanaï and Tajimi
M	Surface magnitude
PGA	Peak ground acceleration
R_d	Hypo-central distance
RPA2003	Algerian seismic regulations
SE	Site effects
SFS	Soil–foundation–structure
SSI	Soil–structure interaction
SSIE	Soil–structure interaction effects
SWV	Shear wave velocity
TF	Transfer function

✉ Mohamed Beneldjouzi
mbeneldjouzi@usthb.dz

Mohamed Hadid
hadidmohamed13@gmail.com

Nasser Laouami
nlaouami@cgs-dz.org

Mustapha Remki
musremki@gmail.com

[1] Water, Environment, Geo Mechanics and Structures Laboratory (LEEGO), Faculty of Civil Engineering, University of Science and Technology Houari Boumediene (USTHB), BP 32, El Alia, Bab Ezzouar, 16111 Alger, Algeria

[2] Transport Engineering and Environment (TPiTE) Laboratory, National High School of Public Works (ENSTP), 1, Rue Sidi Garidi, Vieux Kouba, 16051 Alger, Algeria

[3] Earthquake Engineering Applied Research Centre (CGS), Rue Kaddour Rahim, BP 252, Hussein Dey, 16040 Alger, Algeria

1 Introduction

In strong seismicity areas, post-seismic observations still reveal variations in seismic damage within the same zone. Many recent earthquakes dramatically reminded us of the existence and importance of such effects. The Michoacan

earthquake [1], which struck Mexico City in 1985, serves as the best illustration, where geological conditions that resulted in a sedimentary fill resting on rock strongly influenced the movement of the nearby surface soil and significantly contributed to the extent of damage [2]. The presence of the geological contrast between the rock and the immediate supporting soil deposits alters the features of seismic waves, particularly in terms of frequency content and duration. On the other hand, it is widely recognized that the added flexibility offered by the subsoil of a soft nature decreases the overall stiffness of the soil–structure interacting system and, as a result, modifies the structural response, particularly for some structure types.

The seismic excitation experienced by structures is a function of (i) earthquake source effects [3, 4] associated particularly with seismic magnitude, fault rupture mechanism, and fault directivity; (ii) propagating path effects [5], which essentially control changes in the frequency content; and (iii) local effects related to the local geology and topography called site effects [6, 7], in addition to (iv) SSI effects [8, 9] that result due to the presence of the foundation and its flexible supports. In most cases, local SE induce amplification of the seismic ground motion, but in the case of intense shaking, a soil hysteretic damping effect may considerably reduce the free-field ground motion. SSIE produce inertial interaction resulting in inertial forces developed within the structure due to the existence of structural and foundation masses. Additionally, as the seismic shaking intensity controls the structural response in its FB and rigid foundation conditions, the same observation would be expected in the case of site and flexible-base conditions. Frequently, SE increase the structural response while SSIE can either increase or reduce it depending on the site soil nature and the level of damping.

Building seismic codes consider SE through site factors, which reflect the amplification of seismic waves because of the change in the geological contrast between the rock and nearby supporting soil deposits. Most of these codes consider the assumption of a fixed base (FB), corresponding to a fixed and infinitely rigid foundation. This assumption is conservative in terms of the structure's safety, as it is generally accepted that SSIE reduce the strain on the structural parts. However, those effects can be detrimental and may increase structural stresses. When SE are included, a new loading condition is imposed and the overall structure's response is governed by the dominant effect.

Many studies on the dynamic response of structures dealing with SSIE as well as soil conditions have been conducted in recent decades, but most of them were site-specific, i.e., they consider particular and unique site conditions and often arbitrary selected seismic excitations. Few studies on SSIE, including SE, have been conducted as opposed to numerous investigations on SE. A one-dimensional (1-D) propagation model of shear wave velocity (SWV) was used by Aviles and Pérez-Rocha [10] to study site and SSI impacts in the valley of Mexico City. The study shed important light on the significance of both site and SSI effects. Fatahi et al. [11] found that the traditional design process, which only considers local site impacts and leaves out SSI, is unable to ensure the structural stability of mid-rise moment-resistant buildings higher than 5 stories resting on soft soil deposits. Many other studies that address the effects of SSI and soil conditions for particular types of structures and soil were made [12, 13]. On the other hand, the experience shows that local site conditions analysis should be a critical stage in the design process to understand how the expected amplification induced by the change in impedance contrast and the attenuation created by SSI effects will influence one another. The risk of collapsing is substantially lower in that scenario at extremely significant damage and near-collapse performance levels, especially when the SSIE are advantageous, depending on the type of soil and building [14]. Moreover, investigations made by Dutta et al. [15] and Çelebi et al. [16] focused on the influence of SSIE on a few design key parameters of buildings. They concluded that the change in the seismic base shear (BS) response was found to be more amplified for low-rise buildings resting on flexible soils and subjected to particular types of ground motions, while this response may decrease for medium-to-high-rise buildings. Recently, Deoda and Adhikary [17] studied effects of soil amplification and SSIE on a 10-story RC frame building, and concluded that excluding soil amplification and soil–foundation flexibility, predicts lesser displacement and internal forces.

This study investigates site and SSI effects within the more general framework of seismic regulation standards [18, 19], in contrast to most SSI studies that consider unique circumstances and site-specific issues as mentioned above, and associates the earthquake shaking level expressly to depict cases where SSIE are unfavorable. It explores SE combined with SSIE and their impact on multi-story buildings under the influence of seismic magnitude, based on the concept of the rock-to-soil surface transfer function (TF). The combined structural response is evaluated in the frequency domain, based on a global TF. The study focuses on multi-story buildings sitting on hypothetical soil strata whose deposits are categorized following the seismic standard of EC-8 [18]. The selection of low-to-mid-rise building was made according to the corresponding slenderness ratio, which relates the effective structure's high to its foundation dimensions. To examine the seismic response variation due to seismic magnitude impact, the seismic input used in the analyses refers to several incident seismic fields simulated according to the Algerian seismo-tectonic context in which, variable

earthquake intensities varying from moderate to strong are considered. The study's findings are presented in such a way that ratios can be utilized to show how SSIE differ from SE in terms of their impact on seismic BS and roof displacement.

2 National Seismic Context and Regulatory Seismic Design Considerations

Algeria is classified into four seismic regions, with activity ranging from weak to moderate in the southern and high plateau regions, and from moderate to strong in the northern region [20]. The Boumerdes earthquake (2003, M6.8) was the most recent strong earthquake to occur. Indeed, as shown by recent seismic risk studies [21], northern Algeria is situated near the meeting boundaries of the continental plates of Africa and Eurasia and exhibits considerable geodynamic activity. Many sites in this area show geotechnical, topographic, and geological conditions leading to the rise of local SE. Several studies denoted the presence of SE in active seismic areas [22–25]. The amplification phenomenon is indirectly taken into account in the Algerian Seismic Regulations (RPA2003) [26] through normalized response spectra matching to four soil classes (Table 1). However, the design spectra do not properly integrate the site factor concept, although they reflect several site categories. Beneldjouzi and Laouami [27] proposed a new method for modeling SE based on a mean rock-to-site surface TF for each RPA99 site class. The proposed TFs were used to propose an appropriate seismic site classification. Mean site factors were also calculated for each site class. For structural seismic design, the provisions assume structures with a FB corresponding to a rock site, and no indication is provided regarding SSI analysis.

Table 1 RPA2003 site categories

Site type	Geotechnical description	Mean value of V_s (m/s)
S1	Rock site: Rock or other similar geological formation	$V_s \geq 800$
S2	Stiff site: Deposits of dense sand, gravel, and/or over-consolidated $V_s \geq 400$ clay with 10 to 20 m thickness from 10 m depth	From 10 m depth
S3	Soft site: Deep deposits of medium dense sand, gravel, or medium raid clay	$V_s \geq 200$ from deep of 10 m
S4	Very soft site: Deposits of released sand with/without the presence of soft clay	$V_s \geq 200$ in the first 20 m

3 Study Purpose

Most seismic codes commonly propose site classification schemes based on the local geology of the underlying subsoil and the mean value of SWV in the upper 30 m, in agreement with several related pioneering works [28–31], and provide mean site factors associated with average design response spectra. Several of these codes assume the assumption of a FB corresponding to a hard rock site. Additionally, simplified SSI analysis methodologies are implemented in some of these codes [18, 19], referring particularly to period and damping ratio lengthening along with reduction terms of seismic BS and spectral acceleration.

The RPA2003 (currently under revision) suggests a site classification scheme based on the mean SWV at 10 m depth associated with a geotechnical description of the immediate subsoil background (Table 1). Instead, most modern seismic codes utilize mean SWV at 30 m depth, or $V_{s,30}$, as an effective criterion to offer accurate soil classification schemes [32]. Thus, the EC-8 site classification methodology is used in this study as an alternative for the RPA2003 one (Tables 1 and 2), given the concordance between the EC-8 and RPA2003 classification schemes in terms of surface geology description and SWV arrays.

On the other hand, site factors reflect the ground motion amplification for the outcrop condition, due to the change in the geological contrast between the bedrock and less dense soil deposits close to the soil surface [33, 34]. The type of soil deposits supporting the superstructure and its foundation usually affects the dynamic properties of the soil–foundation–structure (SFS) interaction system by providing it with additional flexibility. In addition, the presence of rigid bodies in the foundation causes a base slab averaging effect [35] to develop at the soil–foundation interface, as well as radiative damping brought on by the

Table 2 One-layer soil data considered in the soil profile simulation and the seismic analyses

Site class		$V_{S,30}$ (m/s) (EC-8)		Density ρ (Kg/m3)	Poisson's coefficient ν
EC-8	RPA2003*	Min	Max		
Bed rock		1500	1500	2200	0.25
A	S1	800	1500	2000	0.30
B	S2	360	800	2000	0.35
C	S3	180	360	1800	0.40
D	S4	100	180	1800	0.45

*RPA2003 site classes are included to establish the correspondence with EC-8 classes

retransmission of a part of the seismic energy from the structure to the ground. This results in an additional damping mechanism and constrains the ground seismic motion to deviate from the free-field motion.

The main goal of this paper is the assessment of the dynamic response of coupled soil–structure systems associated with SE, where the latter are reflected in rock-to-surface TF derived for each EC-8 site category. The concept of TF is employed to derive the response of coupled SFS systems in the frequency domain through a relevant global TF accounting for both SE and the interaction between soil, foundation, and structure. As well, consideration of the impact of seismic magnitude is considered and highlights the influence of the seismic demand features on SE and SFS responses, particularly the seismic BS and roof displacement. The seismic magnitude range selected includes magnitudes M = 5, 6, and 7, and reflects low-to-medium, medium, and high seismic intensity areas, respectively.

Following the EC-8 provisions, we should take into account the magnitude of the earthquakes that contribute mainly to the seismic hazard defined for the probabilistic assessment of the hazard rather than conservative upper limits. Hence, two seismic levels are retained depending on the seismic sources via the corresponding magnitudes and on the epicentral distance effect. The first one corresponds to ground motions arising from earthquakes having a surface wave magnitude greater than 5.5, while the second relates to earthquakes whose surface wave magnitude is less than or equal to 5.5. According to this methodology, it has been considered that the seismic magnitude range retained for this study accurately extends the dominant seismic activity now present in Algerian territory, in agreement with recently compiled earthquake national catalogs [20, 36] (Fig. 1).

4 Soil Site and Structure Modeling

4.1 Soil Model

The EC-8 site categories are represented through fictitious soil profiles using a stochastic simulation approach. Samples of 1500 one-layer soil profiles arising from the 1-D model of the SWV profile have been generated for each EC-8 site class (except E and F classes). A probabilistic model [37] based on random field theory (Eq. 1) was used to generate the EC-8 compliant bounded SWV values in each profile (Eq. 1) (Table 2). Engineering rock-to-soil surface TF of each profile is calculated for dynamic SSI analysis. Figure 2 shows the mean TF of each site class corresponding to low-strain soil shear modulus.

$$V_i^j = V_{i\,\min}^j + \frac{1}{2}\left(V_{i\,\max}^j - V_{i\,\min}^j\right)\left[1 + th\left(s\frac{\Delta v_i^j}{2\pi}\right)\right] \quad (1)$$

where $V_{i\,\min}^j$ and $V_{i\,\max}^j$ are the minimal and maximal bounds of the average SWV in the ith layer of the jth soil profile, respectively; th(.) is the hyperbolic tangent; Δv_i^j is a local and standard random field having zero mean and unit variance, and s is a factor governing the mean SWV variability between its two bounds.

Furthermore, it is commonly accepted that soil deposits behave non-linearly near the surface under strong seismic motions. Mechanical soil properties, mainly elastic shear modulus, G, and damping ratio, β, control the ground's response to cyclic loads. High levels of dynamic loading generate large deformations in underlying soil deposits and induce, respectively, a decrease in shear modulus and an increase in soil damping ratio due to energy dissipation of a hysteretic nature. Low deformation levels (10^{-3}%) cannot capture dynamic property variation [38], which generally originates as a result of medium-to-high seismic stress. Fundamental works provided dimensionless shear modulus and damping curves of adjusted G and β with various strain amplitudes, particularly for sand and gravel soils, to capture strain-dependent values of G and β properties [39–43]. Recent more developed models that take into account effective vertical and confining pressures [44–46] allow for more accurate seismic site analyses. Such models are still applicable to particular soil types, but they might not always be realistic when site regulatory constraints are included.

Instead of using suitable nonlinear soil models, shear modulus and damping curves of adjusted G and β are widely employed to reproduce soil nonlinear behavior through an equivalent linear process. However, due to the limitations of this approach to capture the complex soil response, particularly under high-loading conditions, the methodology provided by the ASCE7-16 standard was adopted in this study. According to this methodology, effective SWV ratios, effective shear modulus ratios, and soil hysteretic damping ratios are presented inside tables, depending on the ground shaking level and site class (Fig. 3).

In Fig. 3, S_{DS} represents the maximal 5% damped design spectral acceleration at short periods. S_{DS} is the design spectral acceleration and represents two-thirds of the maximal 5% damped spectral acceleration at short periods, S_S, following the US national seismic zoning maps which arise from site-specific seismic studies. The ASCE7-16 methodology is utilized because of its good compliance with EC-8 in terms of site classification schemes and

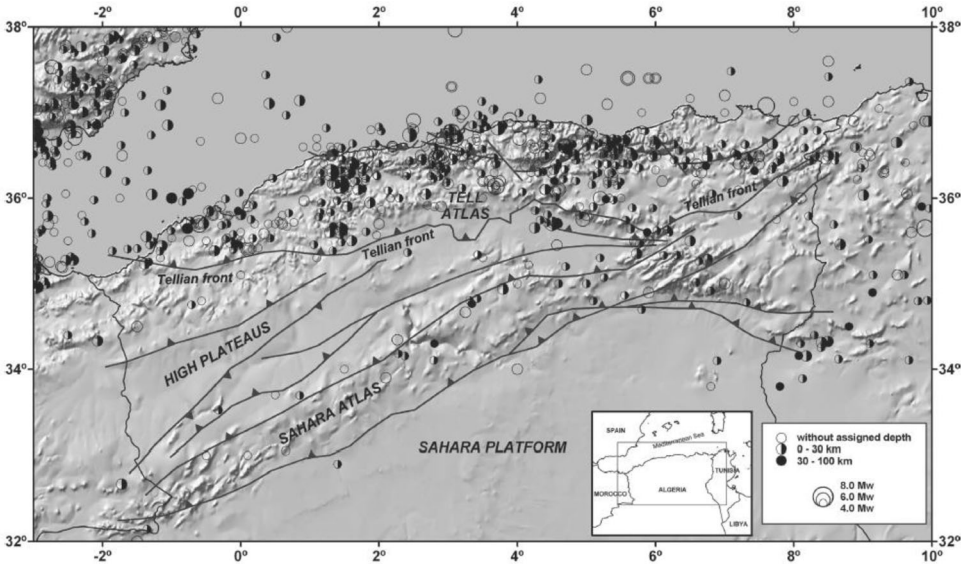

Fig. 1 Seismicity of Algeria and surrounding regions with regional tectonic setting according to Hamadache et al. [36]

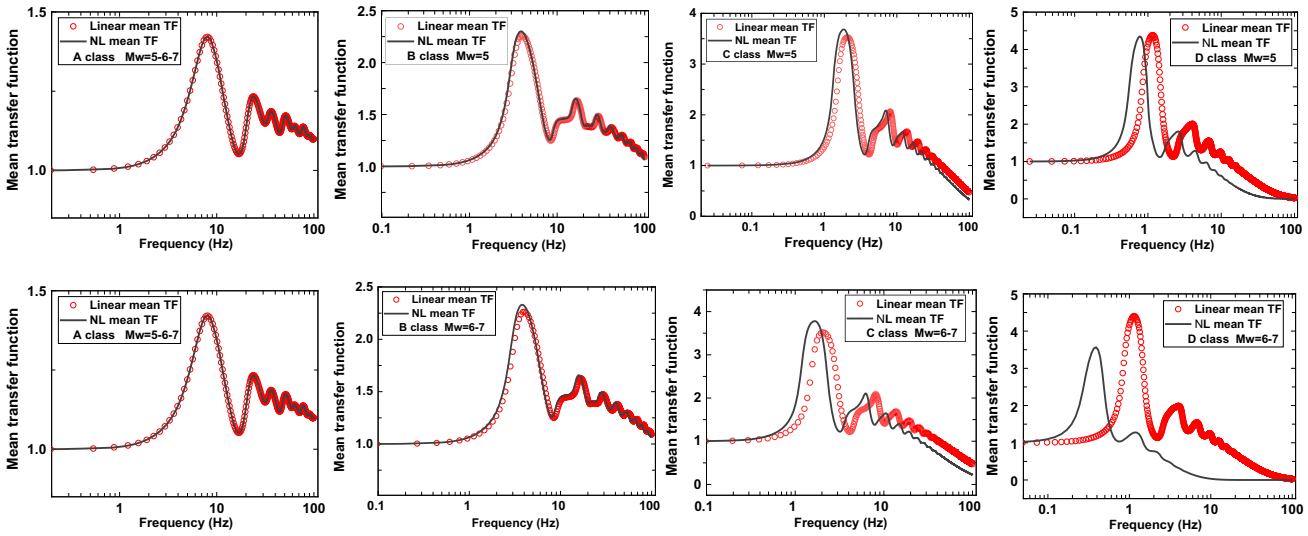

Fig. 2 Linear and nonlinear mean TFs of one-layer profiles representing the EC-8 site classes. Only nonlinear TFs are used in the study, as one plans to emphasize the seismic behavior of buildings. The nonlinear effect is denoted, particularly for strong ground shaking (M6-7 magnitudes) through decreasing the amplification level and shifting the site's natural frequency to the low-frequency range

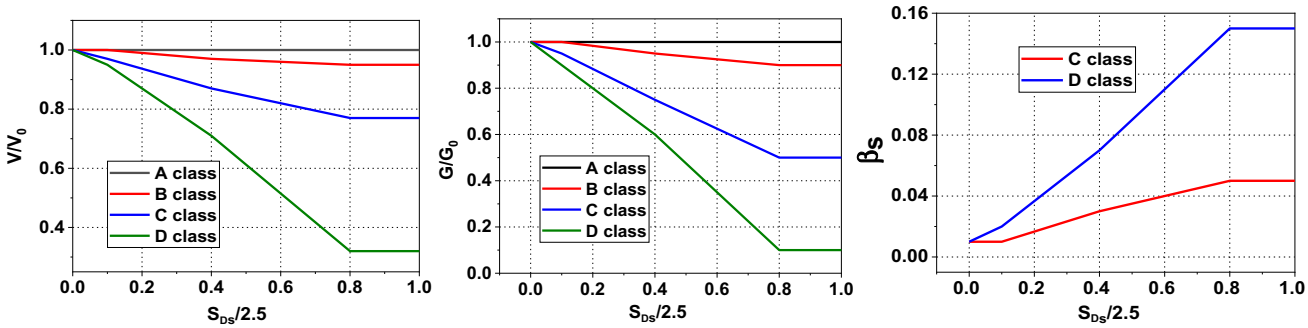

Fig. 3 Reducing G, V_s, and increasing β ratios proposed in the ASCE7-16 standard according to the soil shaking level represented by the maximal 5% damped design spectral acceleration at short periods and site category

with the approach adopted, which deals with different seismic levels.

The S_{DS} used in the study is derived from the rock-site seismic simulation described in Sect. 5, and it represents the maximum 5% damped spectral acceleration chosen from response spectra of all simulated accelerograms based on the regulatory mean prediction shape of Fig. 4. The soil amplification was included through the soil TF instead of site coefficients as in the ASCE7-16 standard. The study's analyses also produced identical G, Vs, and β ratios for the A class across all magnitudes, but distinct ratios for M5 and M6-7 magnitudes were calculated for the other classes.

The TF curve of a one-layer soil profile shows a first peak related to the soil's fundamental mode and secondary peaks corresponding to the soil's higher modes (Fig. 5). In this study, interest is focused on soil response around its fundamental mode, and higher modes of the soil's TFs are ignored, in agreement with structural first mode-based models considered in common SSI problem analyses [9, 47]. For this purpose, the approach of Hadid and Afra [48] dealing with the Kanaï [49] and Tajimi (K&T) model [50] (Eq. 3) was used. The model allows generating a filter having a single mode, which catches the corresponding TF curve accurately (Fig. 5). For each soil profile, the associated TF is used to extract the filter's parameters, mainly the ground resonant circular frequency and total damping ratio. The damping ratio ξ_g, and the circular frequency, ω_g, are evaluated as follows:

$$\xi_g = \frac{1}{2\sqrt{S_{\max}^2 - 1.15}} \text{ and } \omega_g = \frac{2\xi_g}{\left[(1+8\xi_g^2)^{\frac{1}{2}} - 1\right]^{\frac{1}{2}}} \tag{2}$$

where S_{max} designates the peak value of the amplification's function amplitude, taken as equal to the maximum amplitude of the related TF, and corresponds to the fundamental frequency of the soil profile. Replacing the calculated ξ_g and ω_g in the K&T filter (Eq. 3), we obtain an amplification function identical to the calculated TF upstream to the TF fundamental peak (Fig. 5).

$$|H(\omega)|_g^2 = \frac{1 + 4\xi_g^2 \left(\omega/\omega_g\right)^2}{\left[1 - \left(\omega/\omega_g\right)^2\right]^2 + 4\xi_g^2 \left(\omega/\omega_g\right)^2} \tag{3}$$

4.2 SFS Model

The substructure technique, which uses a numerical model with elastic springs and viscous dampers to replicate the foundation impedances, is one of the most commonly used modeling approaches to account for SSIE. According to most substructure approach-based SSI models [9, 51–53], Fig. 4 illustrates the retained SFS rheological model, where the superstructure is represented by a single degree of freedom (1-DOF) system with a height h, mass m, stiffness k, viscous damping factor c, and refers to low-to-mid-rise buildings catered for in the study. This system is connected to a circular foundation of radius R. Following the substructure approach, the soil deposits are replaced by a discrete spring-dashpot system described by impedance functions that reflect the stiffness and energy dissipation mobilized during a seismic excitation giving the soil flexibility. In this context, k_x and k_φ are, respectively, the static soil stiffness along the x-axis and around the y-axis, whereas c_x and c_φ, denote, respectively, the viscous damping factor along the x-axis and around the y-axis. The base of the structure is allowed to move with the u_0 value with respect to the free-field motion, and to rotate through an angle φ around the y-axis. The structures are represented by their first modes characteristics, reflecting a 1-DOF system with the properties (mass, stiffness, frequency, and eigenmode) of the fundamental mode, in agreement with the types of buildings considered in the study.

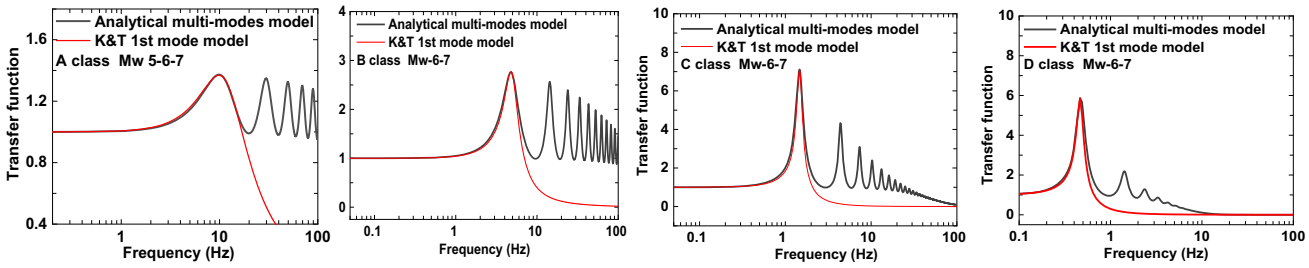

Fig. 4 Typical representations of the TFs related to one-layer profile randomly chosen within the sample of soil profiles considered in the study, along with their corresponding single-mode TFs derived based on the K&T spectrum for the EC-8 site classes. The curves show a match between the two functions up to the first amplification peak. Note that TFs assuming the behavior of soil materials depending on the ground shaking level are represented herein as mentioned in Fig. 2

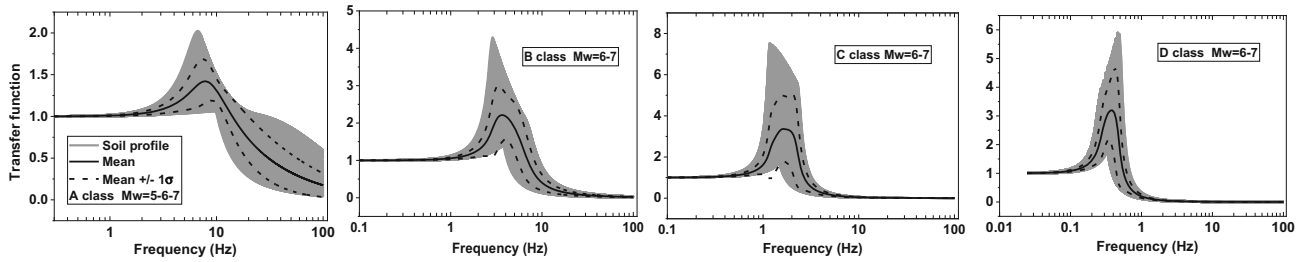

Fig. 5 TFs curves of the simulated 30-m one-layer soil profiles of each EC-8 site class referring to the adjusted $V_{s,30}$ values based on the ASCE7-16 adjusting ratios, including the mean TF and the mean TF ± 1 standard deviation. Only TF graphs corresponding to the 6–7 magnitudes are represented to show the distribution of the TFs curves relative to the related mean curve

5 Seismic Input Motions

Northern Algeria is located in the most active seismogenic area in the western Mediterranean region. The seismicity distribution is represented by four (04) seismic areas (Fig. 1), seismic zones IIb and III for moderate to strong activity, and I and IIa for weak to moderate ones. During the last three decades, northern Algeria experienced several moderate-to-strong earthquakes, two of them were strongly destructive. The 1980 El Asnam earthquake (M7.3), which claimed over 2700 lives and destroyed about 60,000 housings, and Boumerdes May 21 (M6.8) caused considerable damages and claimed over 2300 lives.

According to the Algerian seismic zoning map (RPA2003), we assume for zones I, IIa-IIb, and III, defined by low, moderate, and high seismicity levels respectively, the following magnitude–distance seismic scenarios: M = 7, R_d = 15 km for zone III; M = 6, R_d = 15 km for zones IIa and IIb, M = 5, R_d = 15 km for zone I. The seismic scenarios, in terms of acceleration elastic response spectra, are generated for the three seismic zones, using the recent ground motion prediction equation developed for Algeria and surrounding areas [54] (Fig. 6).

Three sets of 100 spectrum-compatible accelerograms are simulated for the three scenarios considered (Figs. 7 and 8), through an iterative procedure [55, 56] with the following formula:

$$G(\omega_i)^2 = \frac{4\omega_i S_{vi\,(\xi=0)}^2}{\int_0^T a^2(t)dt} \tag{4}$$

where $G(\omega_i)$ indicates the Power Spectral Density of the targeted process at the frequency ω_i, and T, the total duration of the signal. S_{Vi} is the pseudo-velocity spectrum with zero damping derived from the ground motion prediction equation (GMPE) developed for Algeria and surrounding areas for the three scenarios, and a(t) designates a time modulation function proposed by Jennings et al. [57]. Shinozuka's simulation model [58] is used to generate time amplitudes of the accelerogram following the series:

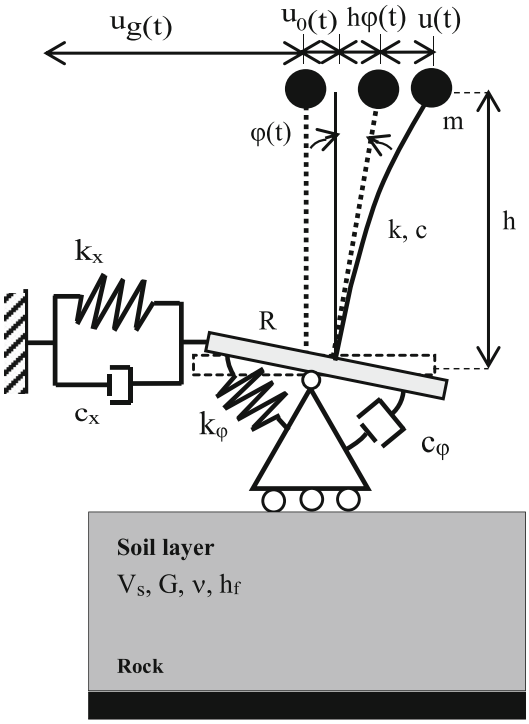

Fig. 6 Simplified modeling of coupled dynamic SFS system for horizontal and rocking modes. V_s, G, ν and h_f stand, respectively, for the mean SWV, shear modulus, Poisson's ratio, and thickness of the soil layer resting on a rock basement. The thickness of the soil layer is taken equal to 30 m to meet the requirements of the EC-8 code

$$\ddot{x}(t) = 2\sum_{k=1}^{n} \sqrt{G(\omega_k)\Delta\omega}\cos(\omega_k t + \phi_k) \tag{5}$$

with $\ddot{x}(t)$, the time-dependent acceleration, and ϕ_k, the random phase angles.

Figure 8 shows peak ground accelerations (PGA) for the three simulated scenarios (M = 5, M = 6, M = 7) and a hypo-central distance R_d = 15 km. From the plotted curves, the three seismic zones considered in this study have low, moderate, and high PGA, respectively. Nonlinear soil behavior should be taken into account, at least for the seismic zone related to the high PGA. The response

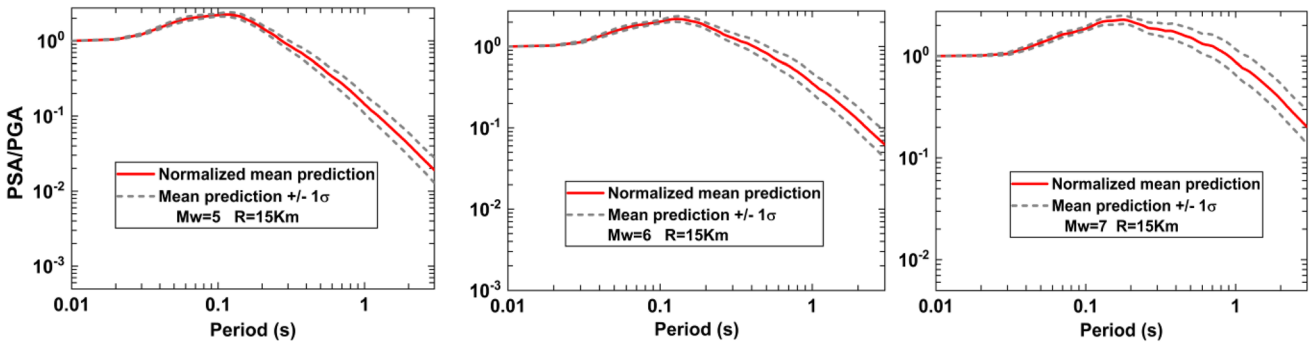

Fig. 7 Predicted peak ground acceleration and spectral acceleration with an epicentral distance of 15 km for M = 5, 6, and 7 reverse faulting earthquakes at a rock site

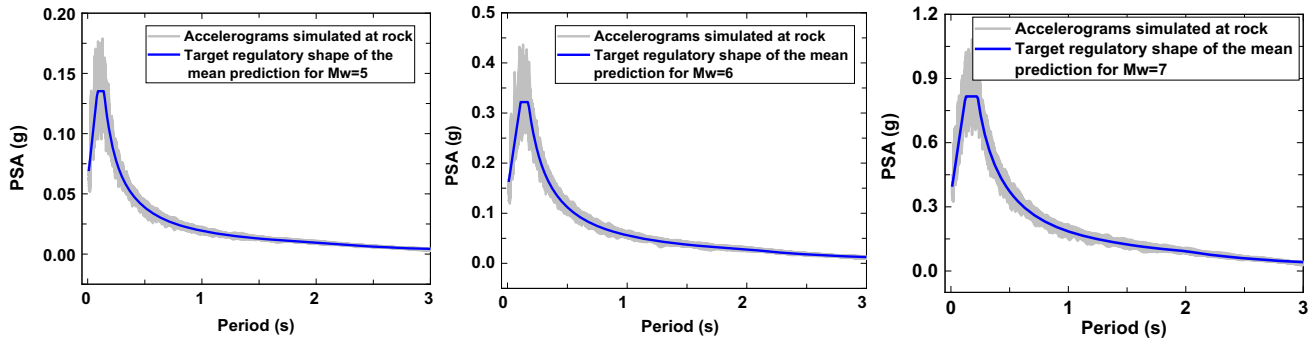

Fig. 8 Response spectra of spectrum-compatible accelerograms simulated according to the GMPE developed for Algeria at the hard rock condition [54]. The mean predictions curves arise from a site-specific study performed based on the selected seismic magnitudes and epicentral distance

spectrum for 5% damping is also calculated for each simulated accelerogram, and the greatest peak spectral acceleration at 0.2 s (short periods) is extracted from all response spectra to derive the G, V_s, and β_s adjusting ratios that will be used later in the analysis.

6 Foundation Stiffness and Damping

Impedance functions represent the frequency-dependent stiffness and damping characteristics of an SFS system and reflect the relationship between the soil and the foundation. Solutions for the complex impedance function proposed by Pais and Kausel [52], and Elsabee and Morray [59] are used:

$$K_j^d = K_j^s(k_j + ia_0c_j)\,(1 + 2i\beta_s) \tag{6}$$

where K_j^d is the dynamic impedance function for the j mode, and K_j^s is the static stiffness following the j direction for a circular foundation of R radius, resting on a homogenous soil layer of h_f thickness. K_j^d is a function of the static stiffness, K_j^s, for a rigid foundation on a semi-finite medium. k_j is a term of dynamic stiffness in the j direction depending on the dimensionless frequency, $a_0 = \omega R/V_s$; where ω is the circular frequency. c_j is the damping factor for the j mode. The term at the right of Eq. 6 is introduced because of frequency-independent internal soil's damping ratio, caused by hysteretic losses due to nonlinear behavior, which is significant around the fundamental frequency of the layer in the case of a soil

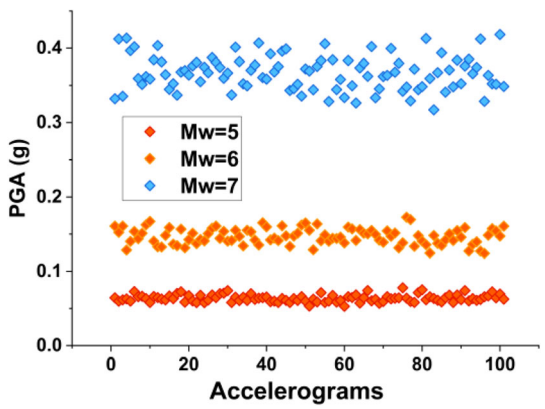

Fig. 9 Seismic input motions represented through the PGA of the accelerograms simulated for the seismic magnitude range selected for the study

layer of finite depth [59, 60]. Static impedance solutions for the system of Fig. 9 are taken as follows:

$$K_x^s = \frac{8GR}{(2-\nu)}\left(1+\frac{R}{2h_f}\right) \tag{7}$$

$$K_\varphi^s = \frac{8GR^3}{3(1-\nu)}\left(1+\frac{R}{6h_f}\right) \tag{8}$$

where G stands for the shear modulus, and ν is the soil Poisson's ratio provided in Table 2 for each site class. β_s is the hysteretic damping ratio of soil materials obtained based on the V_s value for each soil profile according to $\beta_s = 5/V_s$ [61]. G and β_s were adjusted according to ASCE7-16 provisions, based on the site class and maximal 5% spectral acceleration arising from a rock site-specific study.

$$\begin{cases} k_x = 1 \\ k_\varphi = 1 - 0.2a_0 \ if \ a_0 \le 2.5 \\ k_\varphi = 0.5 \ otherwise \end{cases} \tag{9}$$

$$\begin{cases} c_x = \dfrac{0.65\beta_s\xi}{1-(1-2\beta_s)\xi^2} \ if \ \xi = \dfrac{a_0}{a_{01}} \le 1 \\ c_x = c_x^{'} = 0.576 \ if \ a_0 > a_{01} = \dfrac{\pi}{2}\dfrac{R}{h_f} \end{cases} \tag{10}$$

$$\begin{cases} c_\varphi = \dfrac{0.5\beta_s\xi}{1-(1-2\beta_s)\xi^2} \ if \ \xi = \dfrac{a_0}{a_{01}} \le 1 \\ c_\varphi^{'} = 1 - \dfrac{0.35a_0^2}{1+a_0^2} \ if \ a_0 a_{02} = a_{01}\alpha \\ \alpha = \dfrac{V_p}{V_s} = \sqrt{\dfrac{2(1-\nu)}{1-2\nu}} \end{cases} \tag{11}$$

7 Seismic Analysis and Calculation Methodology

The deterministic displacement TF (DTF) is calculated for the consistent one-layer profile, based on the matching small-strain simulated V_s, adjusted according to the ASCE7-16 methodology. Rock acceleration ground motions simulated were used as input motions through a 1-D analysis conducted by a developed computer program for all SWV profiles of each EC-8 site class. The ASCE 7–16 standard's site coefficients taking in account the site amplification effect are included through the soil TF. The dynamic equilibrium of the system in Fig. 4 is given as follows:

$$\begin{aligned} & m\begin{bmatrix} 1 & 1 & h \\ 1 & 1 & h \\ h & h & h^2 \end{bmatrix}\begin{Bmatrix} \ddot{u} \\ \ddot{u}_0 \\ \ddot{\varphi} \end{Bmatrix} + \begin{bmatrix} c & 0 & 0 \\ 0 & c_x & 0 \\ 0 & 0 & c_\varphi \end{bmatrix}\begin{Bmatrix} \dot{u} \\ \dot{u}_0 \\ \dot{\varphi} \end{Bmatrix} \\ & + \begin{bmatrix} k & 0 & 0 \\ 0 & k_x & 0 \\ 0 & 0 & k_\varphi \end{bmatrix}\begin{Bmatrix} u \\ u_0 \\ \varphi \end{Bmatrix} \\ & = -\begin{Bmatrix} 1 \\ 1 \\ h \end{Bmatrix} m\ddot{u}_g \end{aligned} \tag{12}$$

in which $\ddot{u}_g$ designates the harmonic free-field ground acceleration with frequency ω, and m is the first-mode mass of the superstructure. u_0 and u are, respectively, the displacements of the foundation and the mass m with respect to the free-field motion, and φ is the foundation's rocking. k is the structural stiffness whereas k_x and k_φ indicate the dynamic stiffness terms of the soil along the horizontal and rocking directions.

When it comes to harmonic vibrations, the appropriate frequency multipliers can be used to replace the time-dependent derivatives, and by introducing the notations $m\omega_0^2 = k$, $m\omega_x^2 = k_x$ and $m\omega_\varphi^2 = k_\varphi$ the dynamic equilibrium of Eq. 12 transforms to:

$$\begin{aligned} & \begin{bmatrix} \dfrac{\omega_0}{\omega^2}(1+2i\beta)-1 & -1 & -1 \\ -1 & \dfrac{\omega_x}{\omega^2}(1+2i\beta_x)-1 & -1 \\ -1 & -1 & \dfrac{\omega_\varphi}{\omega^2}(1+2i\beta_\varphi) \end{bmatrix} \\ & \begin{Bmatrix} u \\ u_0 \\ h\varphi \end{Bmatrix} = \begin{Bmatrix} 1 \\ 1 \\ 1 \end{Bmatrix} u_g \end{aligned} \tag{13}$$

where β is the damping ratio of the structure with a fixed base; β_x and β_φ relate, respectively, to the damping ratios of the foundation along the x and φ directions:

$$\beta = \frac{c}{2k}\omega_0 \,;\ \beta_x = \frac{c_x}{2k_x}\omega_x \,;\ \beta_\varphi = \frac{c_\varphi}{2k_\varphi}\omega_\varphi \tag{14}$$

According to Wolf [47], the displacement of the structural mass is expressed as:

$$\left[1+2i\beta - \frac{\omega^2}{\omega_0^2} - \frac{\omega^2}{\omega_x^2}\frac{1+2i\beta}{1+2i\beta_x} - \frac{\omega^2}{\omega_\varphi^2}\frac{1+2i\beta}{1+2i\beta_\varphi}\right]u = \frac{\omega^2}{\omega_0^2}u_g \tag{15}$$

thus:

$$u = \widehat{H}\frac{\omega^2}{\omega_0^2}u_g \tag{16}$$

where $\widehat{H}$ designates the DTF stating the SSI which is expressed as:

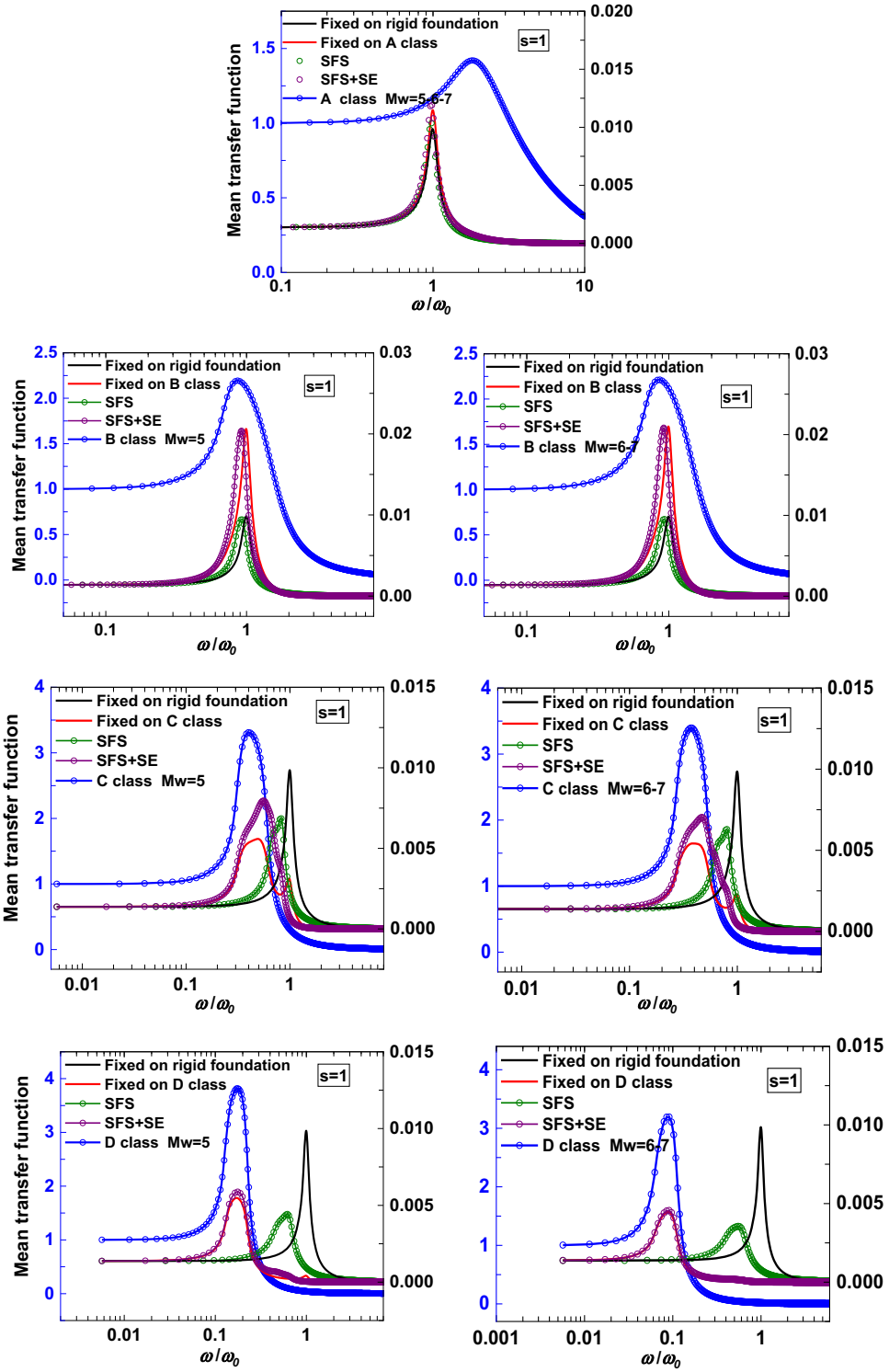

Fig. 10 Average TFs of the s = 1 building's structure in both fixed and flexible base conditions associated with A, B, C, and, D site classes, with M5 and M6-7 magnitudes. The TFs of the sites (in blue) are represented to appreciate their influence on the global response of the SFS system in terms of amplitude and frequency range. In the graphs, FB stands for a structure with an infinitely rigid and fixed foundation, while fixed on soil class represents a structure with a FB subject to SE and changes anticipated to have an impact on the free-field motion without any further flexibility of the foundation soil. SSI and SSI + SE reflect, respectively, the flexible base condition disregarding and including SE. The TFs curves were averaged over the whole sample of the simulated soil profiles

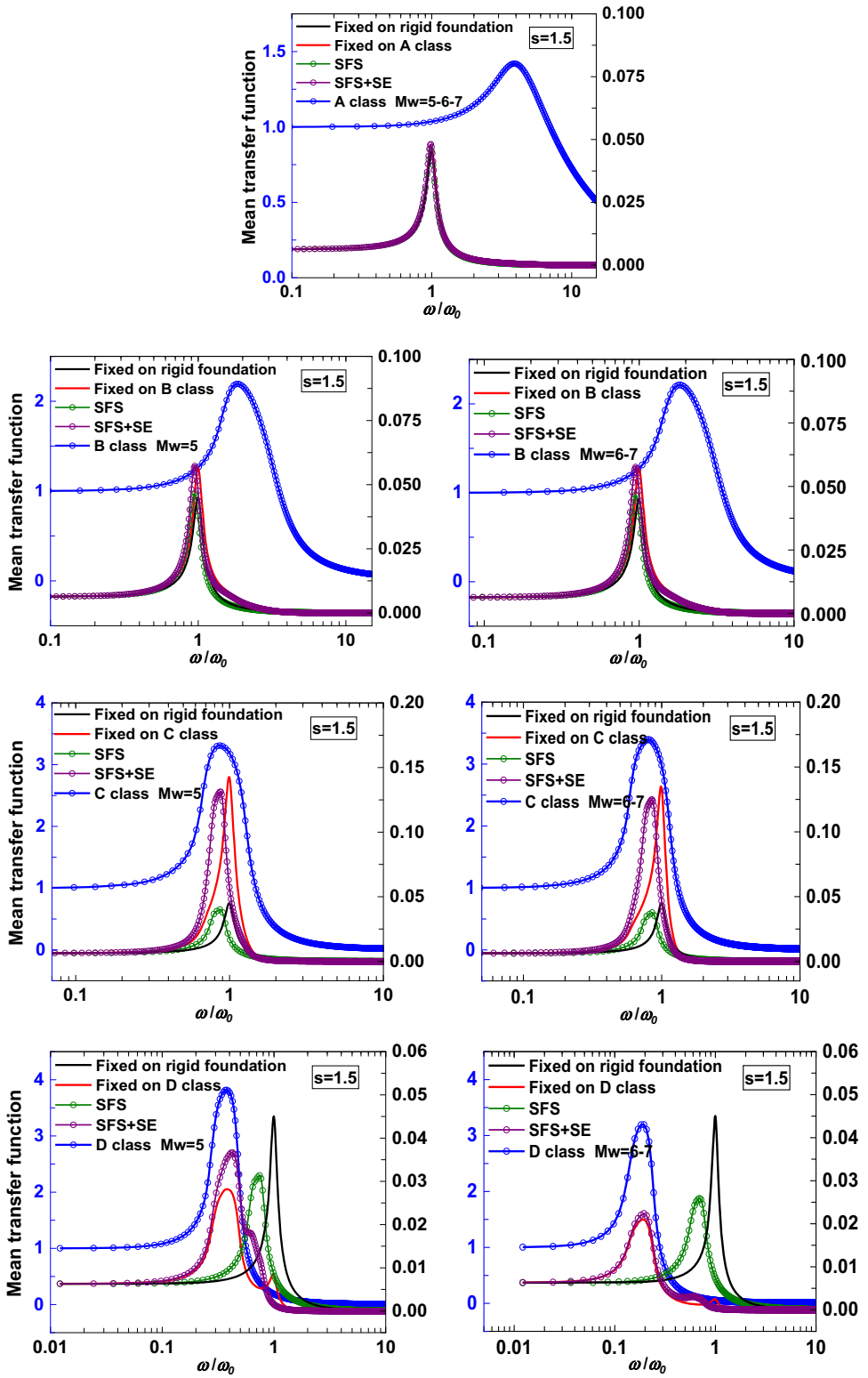

Fig. 11 Mean TFs of the s = 1.5 building's structure in both fixed and flexible base conditions associated with A, B, C, and D site classes. The TFs of the sites are represented to appreciate their influence on the global response in terms of amplitude and frequency range. In the graphs, FB designates the building with an infinitely rigid and fixed foundation, and fixed on soil class, indicates the building with a FB subjected to SE. SSI and SSI + SE reflect, respectively, the flexible base condition disregarding and including SE. The TFs curves were averaged over the whole sample of the simulated soil profiles

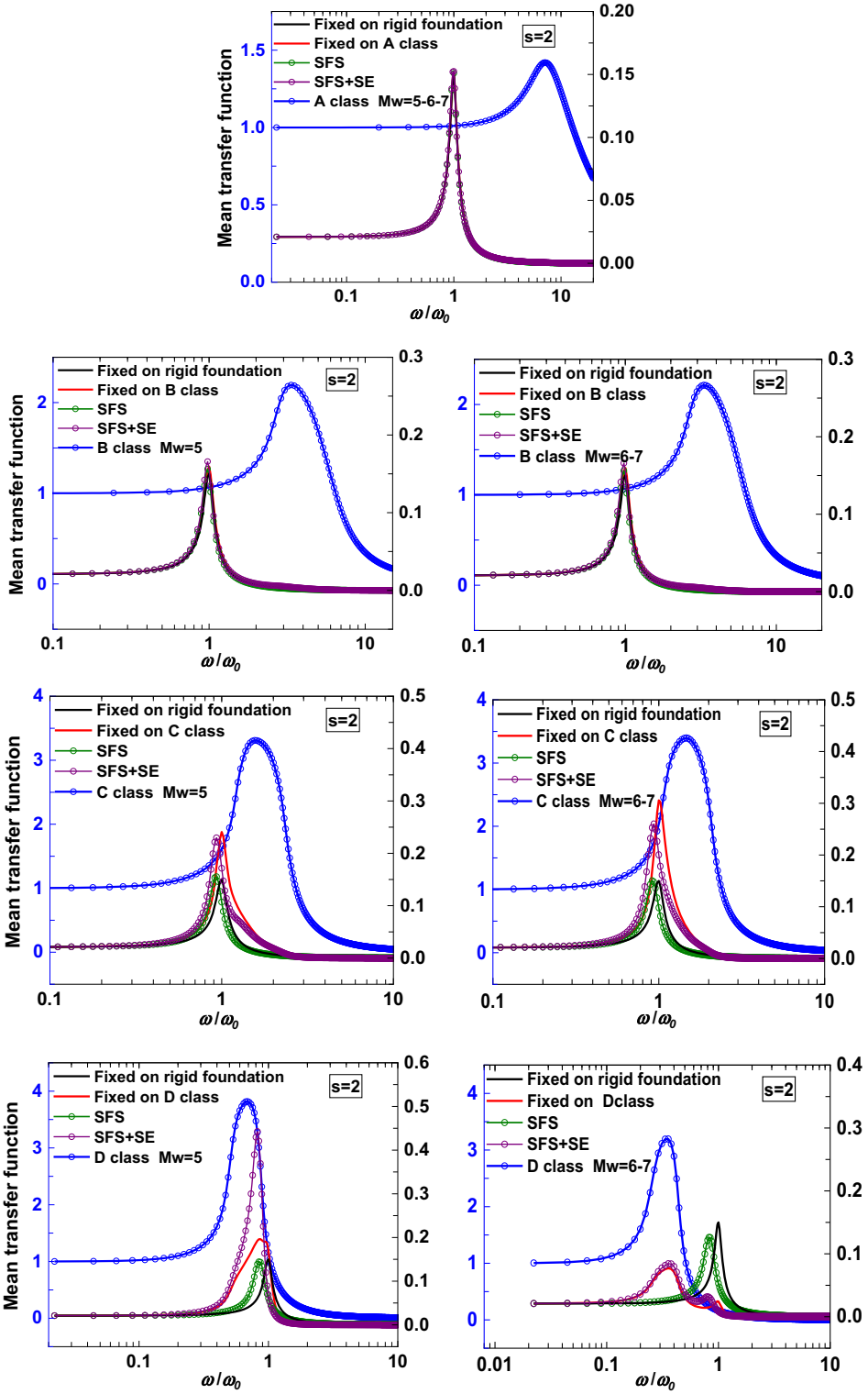

Fig. 12 Mean TFs of the $s = 2$ building structure in both fixed and flexible base conditions associated with A, B, C, and D site classes. The TFs of the sites are represented to appreciate their influence on the global response in terms of amplitude and frequency range. In the graphs, FB designates the building with an infinitely rigid and fixed foundation, and fixed on soil class, indicates the building with a FB subjected to SE. SSI and SSI + SE reflect, respectively, the flexible base condition disregarding and including SE and the flexible base associated with soil condition. The TFs curves were averaged over the whole sample of the simulated soil profiles

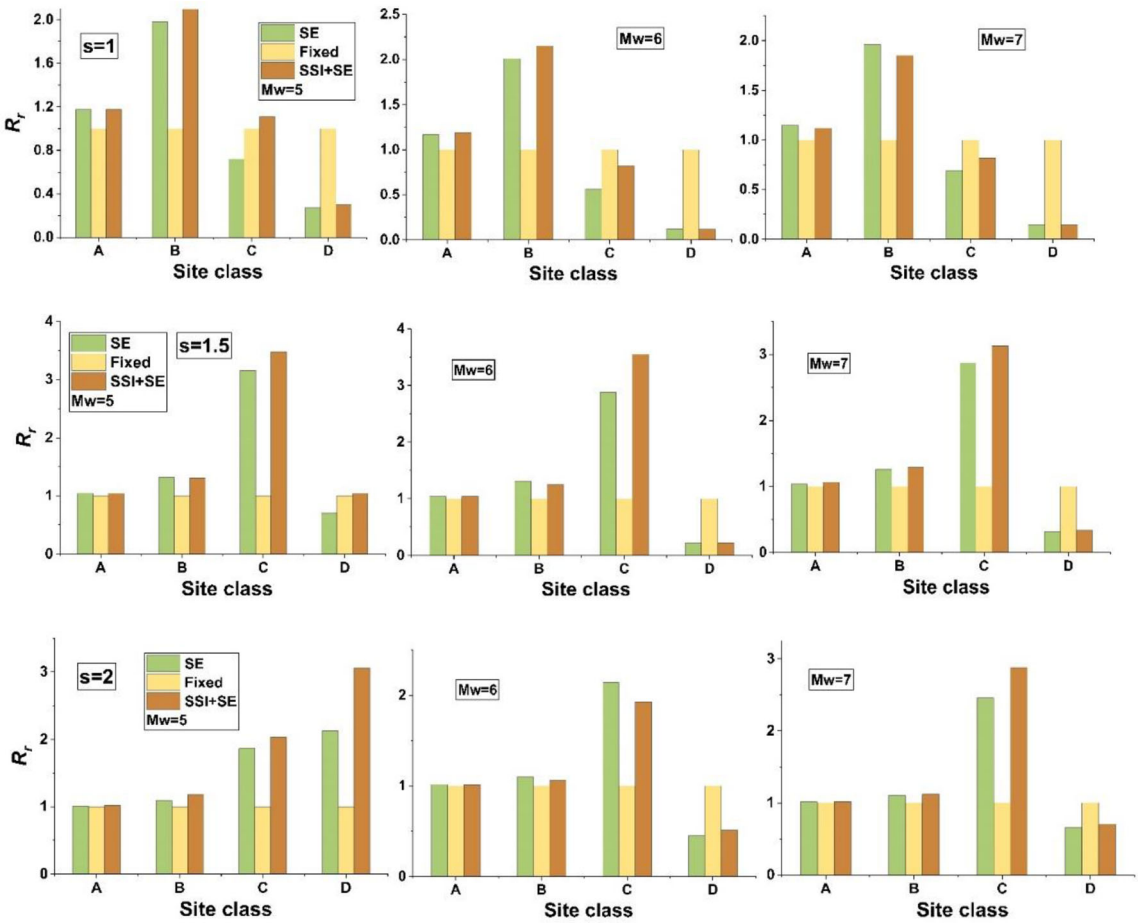

Fig. 13 Response ratio for each EC-8 site class and each building type with M = 5, 6, and 7. The response ratio reflects the mean maximal roof displacement normalized by the FB one and allows for an illustration of fluctuations in the displacement response within the site and site + SSI conditions compared to the FB one, depending on the influence of the incident seismic field

$$\widehat{H} = \left[1 + 2i\beta - \frac{\omega^2}{\omega_0^2} - \frac{\omega^2}{\omega_x^2}\frac{1+2i\beta}{1+2i\beta_x} - \frac{\omega^2}{\omega_\varphi^2}\frac{1+2i\beta}{1+2i\beta_\varphi}\right]^{-1} \tag{17}$$

The system of Fig. 4 may be replaced by a fixed-base equivalent 1-DOF system with natural frequency $\tilde{\omega}$, having the same mass m, equivalent stiffness $\tilde{k}$, and equivalent damping ratio $\tilde{c}$. In this case, the relative displacement of the mass m within the equivalent system is given as:

$$\tilde{u} = \tilde{H}\,\tilde{\ddot{u}}_g \tag{18}$$

where

$$\tilde{H}(i\omega) = \frac{1}{\tilde{\omega}^2 - \omega^2 + 2i\tilde{\beta}\tilde{\omega}\,\omega} \tag{19}$$

and

$$\tilde{\ddot{u}}_g = \frac{\tilde{\omega}^2}{\omega_0^2}\ddot{u}_g \tag{20}$$

$\tilde{H}$ designates the SSI TF of the equivalent 1-DOF system, $\ddot{u}_g$ the acceleration input motion, and $i^2 = -1$. The natural frequency $\tilde{\omega}$ and the damping ratio $\tilde{\beta}$, of the equivalent system are taken equal to the complete analytical solutions provided by Maravas et al. [62]:

$$\tilde{\beta} = A\left[\frac{\beta}{\omega_0^2(1+4\beta^2)} + \frac{\beta_x}{\omega_x^2(1+4\beta_x^2)} + \frac{\beta_\varphi}{\omega_\varphi^2(1+4\beta_\varphi^2)}\right] \tag{21}$$

in which

$$A = \left[\frac{1}{\omega_0^2(1+4\beta^2)} + \frac{1}{\omega_x^2(1+4\beta_x^2)} + \frac{1}{\omega_\varphi^2(1+4\beta_\varphi^2)}\right]^{-1} \tag{22}$$

and

$$\tilde{\omega} = \frac{A}{(1+4\tilde{\beta}^2)} \tag{23}$$

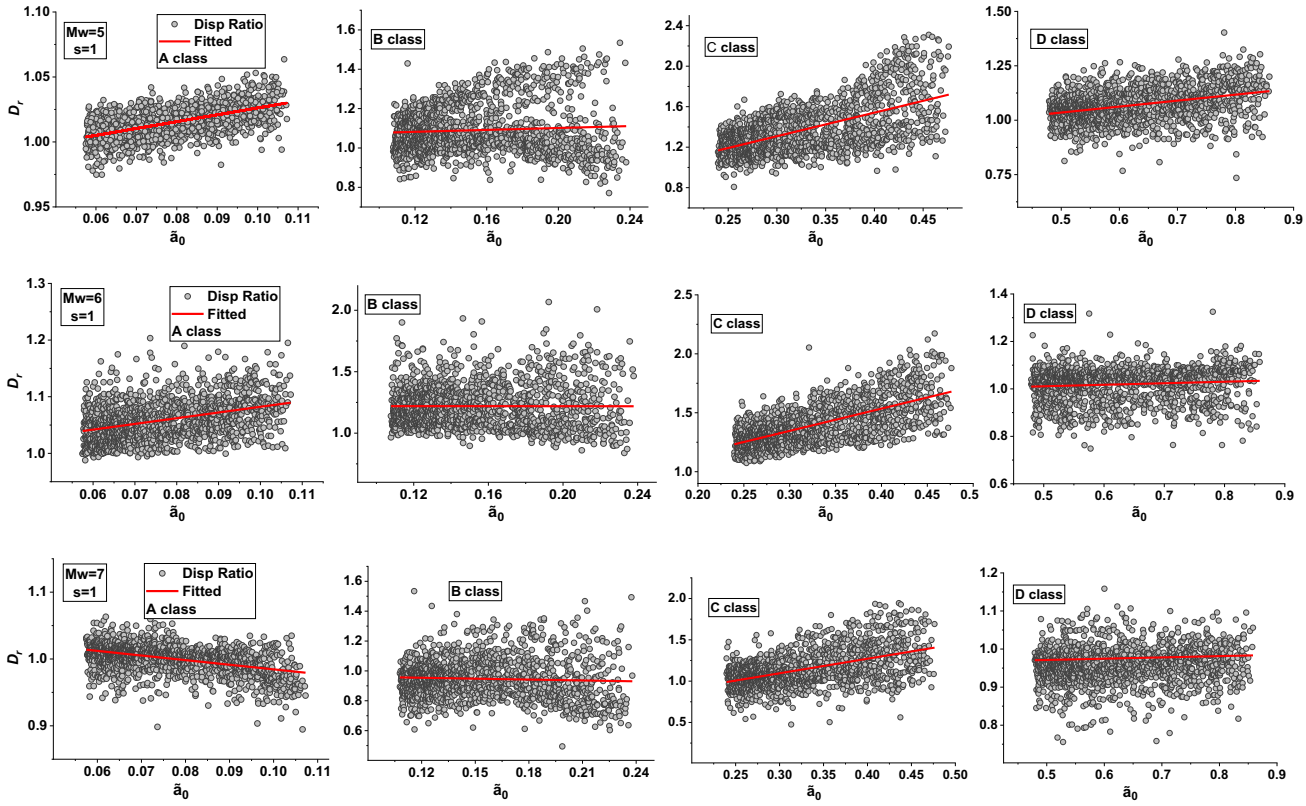

Fig. 14 Displacement ratio versus soil-to-structure stiffness ratio with the best fit for the s = 1 building with M = 5–6-7

On the other hand, nonlinear behavior is anticipated from the superstructure at large earthquake magnitudes. In accordance with the ASCE7-16 formula for effective frequency, the structural ductility is used to account for the material nonlinearity:

$$\left(\frac{\tilde{\omega}}{\omega_0}\right)_{eff} = \left\{1 + \frac{1}{\mu}\left[\left(\frac{\omega_0}{\tilde{\omega}}\right)^2 - 1\right]\right\}^{-0.5} \tag{24}$$

in which μ designates the global ductility of the superstructure and $\tilde{\omega}$, is the natural frequency of the equivalent system. The SSI TF is finally combined with the site TF,H_s, to obtain a global DTF taking into account site and SSI effects:

$$\tilde{u} = \overline{H}\,\tilde{\ddot{u}}_g \tag{25}$$

where

$$\overline{H}(i\omega) = \tilde{H}H_s \tag{26}$$

According to the suggested methodology (Eqs. 12–26), a global TF that takes into account site and SSI effects is obtained by combining the TF for the entire sample of soil profiles related to each site class with the TF of the structure, followed by the resulting one, with the foundation impedance. In each case, the combined TFs over the whole frequency range taken into consideration are averaged to produce a mean DTF for the lateral response (Figs. 10, 11, and 12).

The building types were selected based on the slenderness ratio, s, which relates the effective height of the superstructure to its foundation dimensions. The responses of each building type are carried out for the scenarios of FB and rigid foundation, FB on site class, and flexible base on site class. The results are represented first through a mean displacement TF referring to each condition with all seismic magnitudes. For all site classes, a mean response factor, which is the ratio of the maximum roof displacements for the case of FB compared to the two other conditions, is carried out. To emphasize the fluctuations brought on by taking SFS effects into account, an average response factor for all site classes is calculated by dividing the maximum roof displacements for the case of FB by the two other cases. Additionally, the maximum roof displacement and seismic BS are taken into account for all building types and seismic scenarios across an appropriate range of the structure-to-soil stiffness ratio, $\tilde{a}_0 = h/V_sT_0$, where T_0 denotes the superstructure's natural period. The $\tilde{a}_0$ ratios reflect the variation of SFS system features given a site class according to the change of soil profile mechanical properties. Figures 10, 11, and 12 illustrate the differences between building responses within the cases considered. As well, the results are depicted in the form of

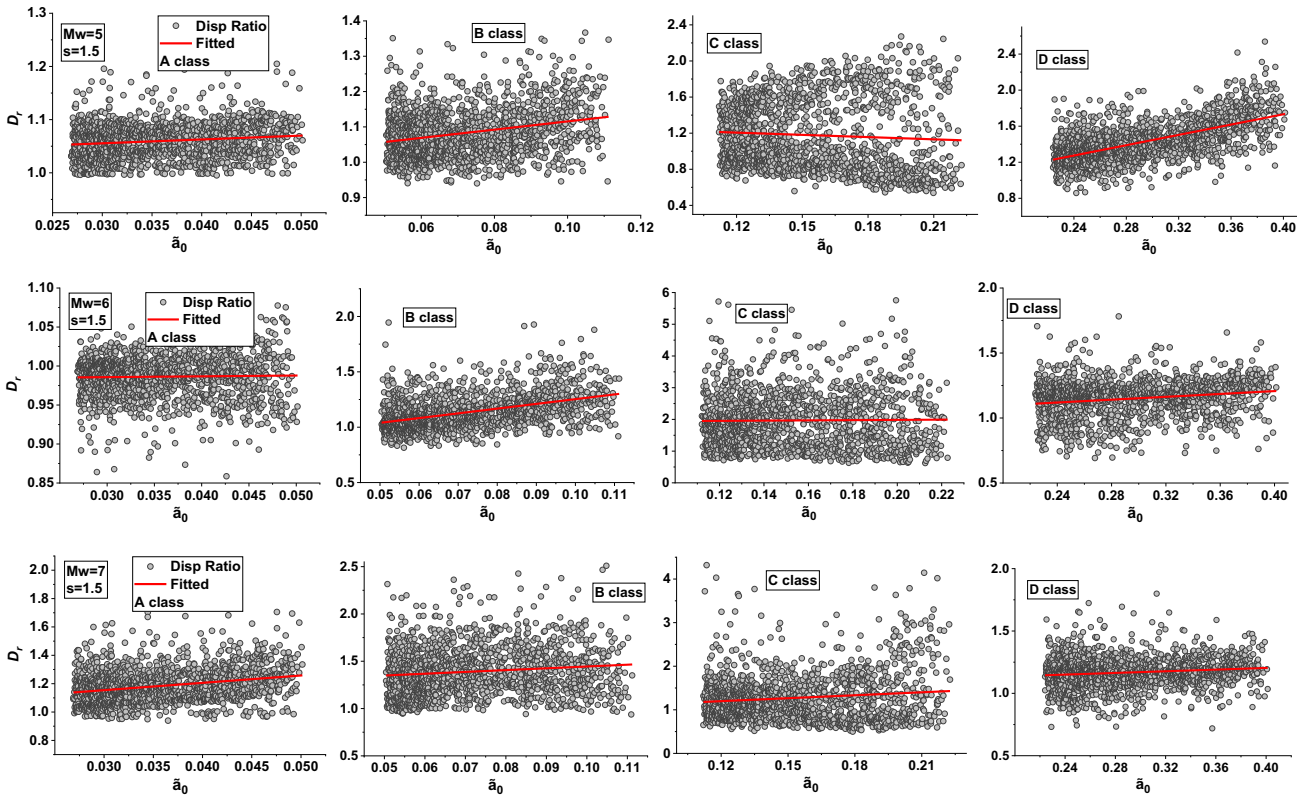

Fig. 15 Displacement ratio versus soil-to-structure stiffness ratio with the best fit for the s = 1.5 building with M = 5–6-7

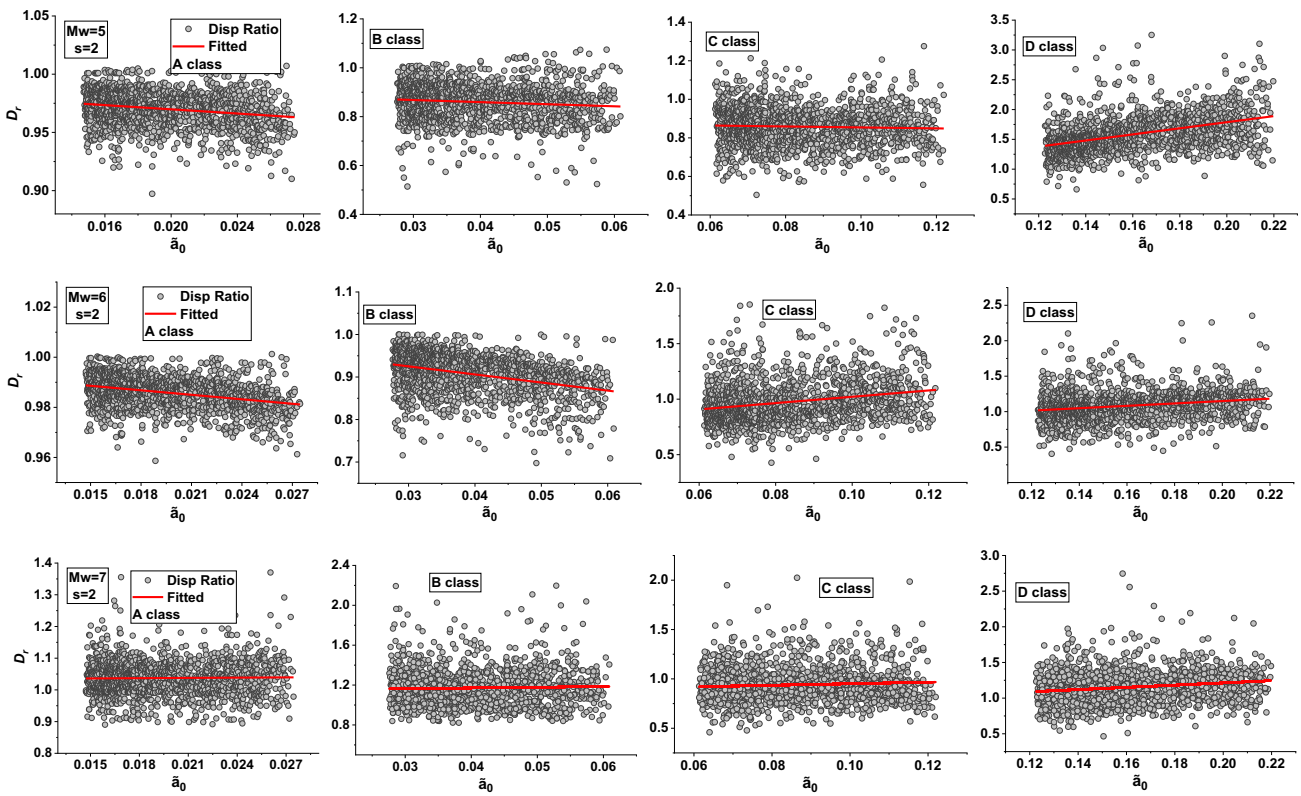

Fig. 16 Displacement ratio versus soil-to-structure stiffness ratio with the best fit for the s = 2 building with M = 5–6-7

mean maximal roof displacement and BS ratios. These ratios are calculated to show the influence of SE on SSIE and vice versa.

8 Results and Discussion

8.1 Displacement Transfer Function

8.1.1 Building with s = 1

Figure 10 shows the lateral DTFs of the building having a slenderness ratio, $s = 1$, and it emphasizes the system fluctuations within the settings taken into account in the study. These TFs are obtained by averaging all related TFs over the frequency range of interest, normalized by the superstructure's circular frequency. In other words, they represent mean curves of all TFs within the range of $\tilde{a}_0$ ratios regarding the building considered. The right-hand side coordinates indicate the amplitude of the combined soil, structure, and foundation DTF, which cannot be directly numerically compared, while the blue left-hand side coordinates represent the rock-to-soil surface TF, indicating a dimensionless amplification ratio for the outcrop condition that derives from the theory of wave propagation in elastic mediums.

Given the results, it is assumed that mean DTFs, which show the same general trend, appropriately represent individual DTFs of SFS systems in terms of amplitude and frequency range (Fig. 9). The graphs show an absence of SSI effects for the building on the A site class, and that such a site class accurately reflects the FB condition. However, a negligible SE looks because of the presence of the structure's natural frequency within the beginning of the ascending branch of the soil TF, and an infinitely rigid base condition may not comply with the real situation.

Due to the lack of nonlinear effects in the B site class, it is clear that no differences related to seismic magnitude exist. In contrast, the TF of the structure with FB on B class exhibits a obvious amplification peak. Although stiff soil deposits typically do not result in high amplification levels, in this instance, the latter reflects the rise of SE as a result of the structure's fundamental frequency being close to the B site dominant frequency. One can infer that structural response is governed similarly by site or site + SSI effects because the TF of the mutual site and SSI effects follows the structure's-site one. Furthermore, SSIE are not substantial even though a little shift toward lower frequencies is detected due to rigid structure on a stiff site.

For the C class, TF curves show the presence of SSIE with amplitude decreasing with respect to the FB condition and a clear offset to lower frequencies because of the system's increased flexibility caused by the C site type. In addition, there is a slight change in the TFs associated with seismic magnitude due to a minor sliding at the low frequencies related to the soil TFs. As well, SE are reduced despite the consistent soil amplification caused by the offset of the related peak TF, and one can retain that structural response is governed by site + SSI effects, whose maximal amplitude is still greater than that of SE.

The building with a slenderness ratio of unity resting on D class reflects the most favorable situation where SSI effects are strongly expected to occur due to the significance of the structure-to-soil stiffness ratio. In line with the characteristics of the D site class, the related SFS system has a lower natural frequency than the system with a FB. In addition, SSIE look beneficial compared to the FB condition, even to SE + SSIE, when SE are disregarded, but the FB condition is conservative and unfavorable for the C and D classes. The effect of seismic magnitude is also clearly discernible for the D class, as a result of nonlinear effects originating with moderate-to-high seismic magnitudes. This have resulted in a more reduced site + SSI response, and made visible the attenuation of the soil amplification related to all magnitudes with shifting to lower frequencies. For all site classes (with less extent for the A class), the site + SSI TF curves show a response that occurs within the frequency range of the soil's fundamental mode, regardless of the response magnitude. This assumes that SFS condition controls the global combined response in terms of amplitude, whereas the soil condition controls the response in terms of the frequency range.

8.1.2 Building with s = 1.5

The TFs curves for the structure with a 1.5 slenderness ratio are shown in Fig. 11. The FB with stiff foundation condition is compatible with the A class's lack of site or SSI effects. Only a very small amount of SE is found for the B class, where no SSIE is associated, and the structural response is controlled by either site or SSI effects that have a similar impact on the structure.

Although SSIE can be seen in the C class with a lower natural frequency effect, they have no actual bearing on the structure's response, and due to the existence of the natural structure's frequency within the frequency range of the soil's amplification peak, these effects are amplified by the high values of the site's TF and help to explain why, in the flexible-base condition, site + SSI effects govern the structural response rather than SE. The relevance of nonlinear effects in high magnitudes, however, results in a variation in soil TFs related to the D site class and causes a damped soil peak amplification with shifting to the lower frequencies. Due to the increased system flexibility provided by the D site type, the building illustrates the instance of a moderately rigid structure over a soft site

where SSIE are present. In the FB condition, the structural response is controlled by SE and is detrimental when SE are ignored, whereas, in the flexible-base one, the response is governed similarly by site or site + SSI effects. Also, the plots further demonstrate that the SFS condition controls the extent of the global response for the C and D classes, whereas soil conditions control its dominant frequency.

8.1.3 Building with s = 2

The TF graphs in Fig. 12 show that a structure with a slenderness ratio of 2 is relatively flexible and free of significant site or SSI effects, notably in the A and B classes. This is caused by the weak values of the soil's TF near the resonant frequency of the structure, which reduces the SSI and site effects coming from upstream of the site's TF peak. The slenderness of the building associated with consistent values of the structure-to-soil stiffness ratio also reveals a weak occurrence of SSIE for the C class. For M6-7 magnitudes, where the peak amplification of the FB TF coincides with the ascending branch of the soil TF peak, SE and therefore, site + SSI effects are dominant. Furthermore, due to nonlinear soil behavior under intense seismic loading, the M6-7 magnitudes provide more damped peak amplification and low-frequency effect. The TF of the site varies with seismic magnitude for the D class. In this regard, the seismic magnitudes result in different responses even for the same site class. Therefore, site + SSI response is strongly pronounced for the M5 magnitude and appears within the amplification peak of the soil's TF, whereas it is significantly reduced for the M6-7 magnitudes due to the low-frequency effect, which causes the soil's amplification peak to be far from the FB one and requires a downward trend in both site and SSI effects away to the natural superstructure frequency, indicating low soil resonant frequency.

8.2 Average Maximal Response Ratio

An SFS system and the corresponding FB one are created for each site soil profile, and both are then subjected to the incident seismic field that was previously simulated for all seismic magnitudes considered. The displacement response at the building roof is carried out in the frequency domain according to the methodology presented above, then converted to the time domain through the Fourier transform, and the maximal displacement corresponding to each ground motion is extracted. As well, the mean maximal displacement is obtained by averaging all maximal displacements for each site soil profile.

Figure 13 shows the influence of the SE and SSI + SE conditions compared to the FB one in terms of response ratio, R_r, depending on the effect of the incident seismic field. R_r denotes the mean maximal roof displacement within the site and site + SSI conditions normalized by the FB one. According to FEMA P-2091 standard [63], a flexible base produces important roof displacement in contrast with FB, and, subsequently, controls the structural damage. The graphs denote agreement with the related TF curves for each EC-8 site class and each building type. As well, the graphs of Fig. 13 show a similarity of the response within the A class, and to a lesser extent, the B class for the $s = 1.5$ and $s = 2$ buildings, whereas no seismic magnitude effect is observed for the $s = 1$ building.

A strong dominance of SE and, consequently, SE + SSIE is observed, notably for the B class due to the correlation between the site and building features for the $s = 1$ building, and implies an underestimation of the response if soil conditions are ignored. The significance of SE and SE + SSIE, is highlighted for all magnitudes for the C class with the $s = 1.5$ and $s = 2$ buildings, where the FB condition underestimates the response, whereas, for the s = 1 building, the total response (SE + SSIE) fluctuates around the FB one. The FB condition overestimates the response for the $s = 1$ building with all magnitudes and demonstrates its conservatism relative to the other conditions. The FB condition displays the same pattern as the TFs curves and overestimates the response for $s = 1.5$ and $s = 2$ buildings in the D class and M6-7 magnitudes (Fig. 11). But for the M5 magnitude, the response is underestimated for the $s = 2$ building and is in the same order as the $s = 1.5$ building.

8.3 Average Maximal Deflection Ratio

The results are shown to emphasize the role of SSIE in comparison to SE for the selected seismic magnitudes and all site classes. The basis for comparison is the ratio of the average maximal roof displacement (and subsequent average maximal BS force) under site and SSI effects. This allows engineers to clearly see whether and when one or the other effect is dominating when it comes to regulatory concerns, especially when the problem also relates to the magnitude of the seismic input. To get the mean maximal displacement ratio, D_r (Eq. 27), between the two conditions for each system, the TFs of the flexible and FB conditions, both of which include SE, are taken into account. This ratio illustrates the situation where SE are removed from the flexible base global response to emphasize the magnitude of the SSI effects while SE are ignored from that response, and whether the response in the former or latter condition is dominant depending on the extent of the seismic excitation.

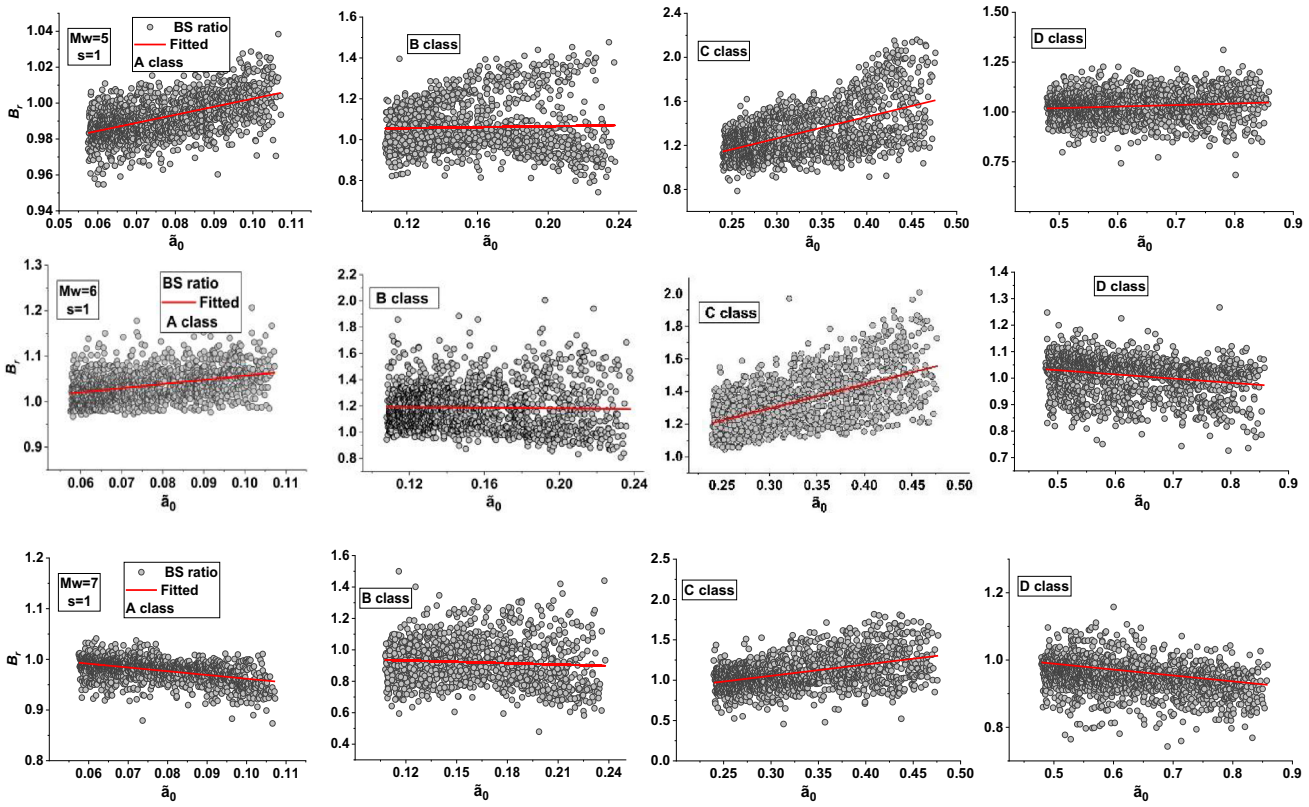

Fig. 17 Base shear ratio versus soil-to-structure stiffness ratio with the best fit for the s = 1 building with M = 5–6-7

$$D_r = \frac{d_{SSI+SE}}{d_{SE}} \tag{27}$$

where d_{SSI} and d_{SE} indicate the mean maximal roof displacement in the SFS and site conditions, respectively.

8.3.1 Building with s = 1

For each class and each magnitude, deflection ratios vs the $\tilde{a}_0$ ratio are shown in Fig. 14, along with the best fit that was achieved using the least square approach. The results in the form of TFs curves are generally in best agreement with the fit curves, which show the results' average trend. According to Tabatabaiefar and Massumi [64], the $\tilde{a}_0$ ratio is the best parameter that controls the occurrence of SSI effects, and the latter are usually met when $\tilde{a}_0 > 0.1$ for buildings with more than 3 stories.

For the A class and the M5 magnitude, the D_r ratio appears to be around unity, indicating that there is no evidence of SSI effects and agreeing with the associated TFs curves (Fig. 10). The correlation between the seismic input features and the flexible base systems with soil conditions is indicated by a modest amplification of the response that is seen around the upper values of $\tilde{a}_0$ for the M6 magnitude owing to SE.

A conclusion that can be drawn from the overall trend of the D_r ratio for the entire soil profiles of the A class is that SE, independent of seismic magnitudes, weakly control the structural response, which may be referred to as the FB condition. Additionally, and for the B class, D_r values that are dispersed to the fit curve, especially for the M5 magnitude and greater $\tilde{a}_0$ values, represent systems with soil profiles that have interacted differently with the seismic input depending on whether their peak amplification is close to or far from the superstructure one. Given the associated TFs curves (Fig. 10) and the minor values of the $\tilde{a}_0$ ratio, SSI effects are typically not significant for this site class. The D_r ratio was close to unity over the entire range of the $\tilde{a}_0$ ratio when the combined site + SSI effects response of the SFS system, on the other hand, showed the same scope with SE around the superstructure resonant frequency. This trend is observed for all magnitudes, except in the M6 one, where seismic input features have a greater impact on the structural response. Additionally, because site + SSI effects response is more significant than SE alone for the C site class, one can conclude that SSI effects govern the structural response. This is especially true for higher values of the $\tilde{a}_0$ ratio, which reflect systems with less overall stiffness due to declining soil mechanical properties.

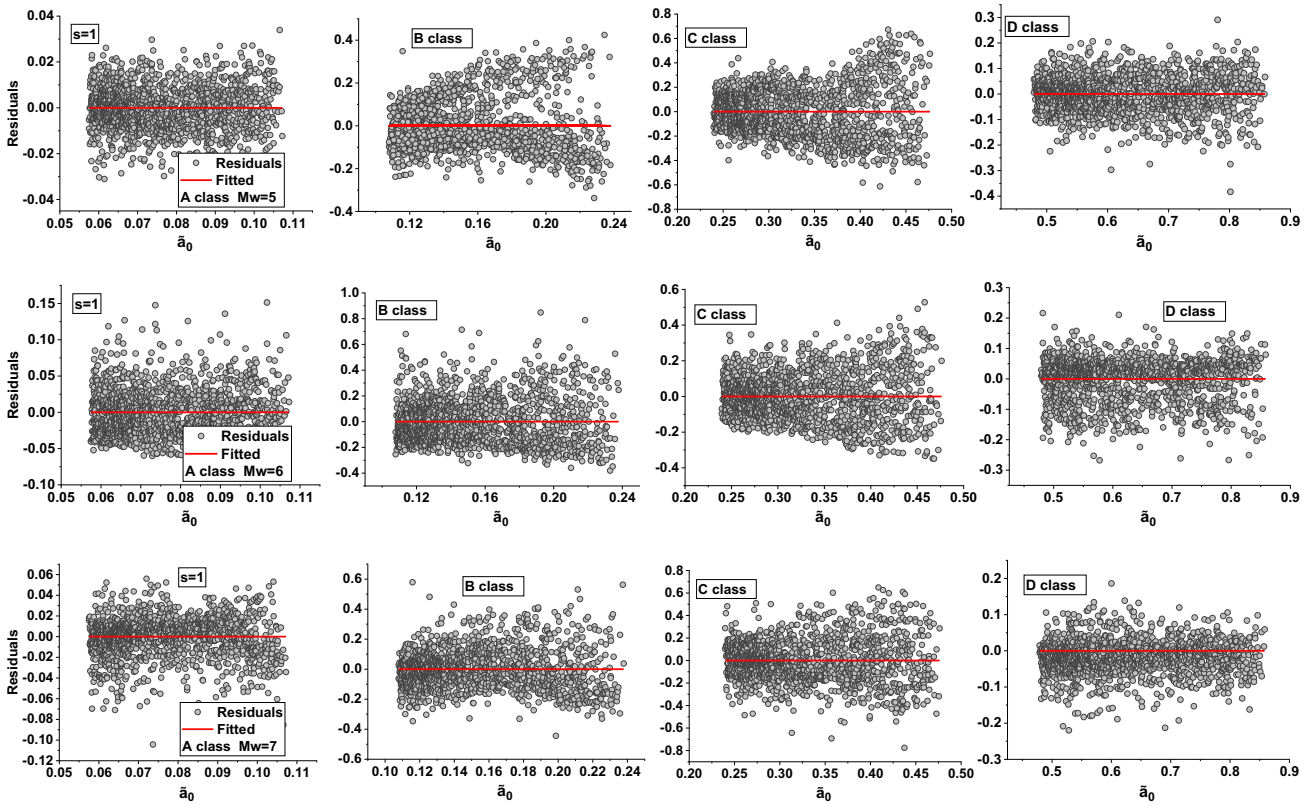

Fig. 18 Residuals versus $\tilde{a}_0$ ratio relative to the corresponding linear regression fit curve of the B_r ratio results related to the $s = 1$ building for all magnitudes and all site classes

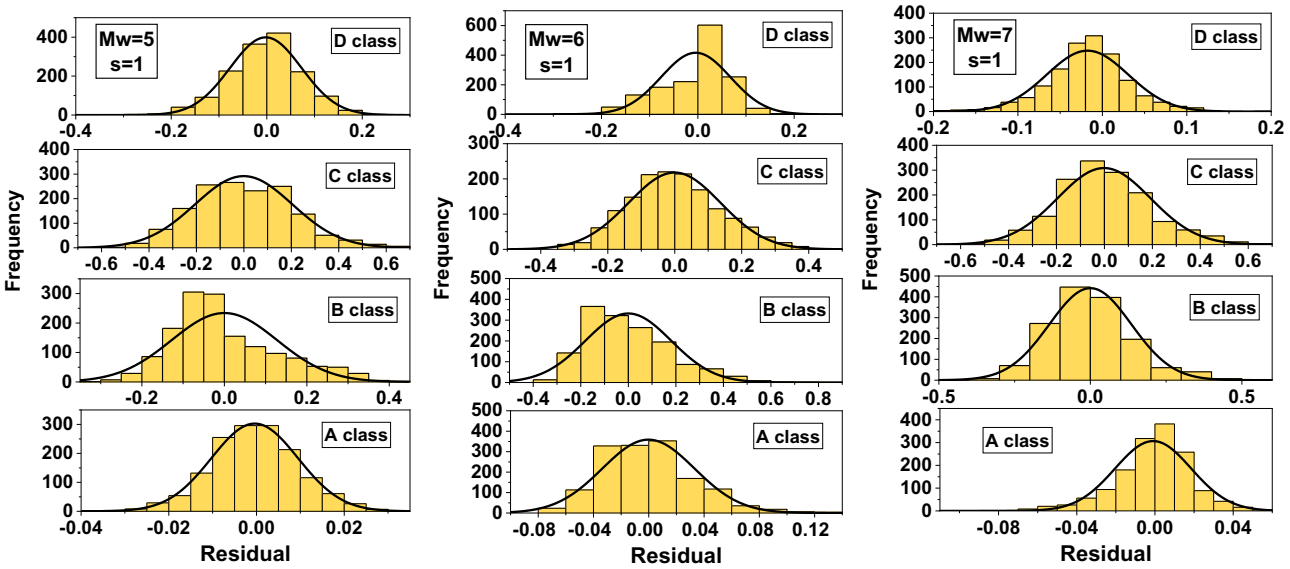

Fig. 19 Distribution of the residuals of the B_r's linear regression model along with the distribution curve of the $s = 1$ building, for all magnitudes and all site classes

In the D class, the combined response is anticipated to be at least comparable to that of the C class for all magnitudes, with SSI impacts being more visible when they are seen alone, especially for this type of building (Fig. 10), due to more important values of $\tilde{a}_0$ ratio. However, attenuation of the response is observed with a reduction of D_r values to about unity, allowing us to conclude that the structural response is either controlled by site or site +

SSIE as a result of nonlinear and low-frequency effects arising in this class type, particularly for the M6-7 magnitudes.

8.3.2 Building with s = 1.5

Similar to the building with s = 1 on A class, no SSIE or SE are dominant and this class can be assimilated to the FB condition for the M5-6–7 magnitudes (Fig. 15). The characteristics of the associated ground motions, whose frequency content situates close to the building's resonant frequency, may also be responsible for the slight increase in D_r that is visible in the M7 magnitude.

Due to the equivalence between site and site + SSI effects demonstrated by the related TF curves (Fig. 11), the D_r values obtained for the B site class and all magnitudes show no signs of SSI effects. This constrains its values near unity mainly for M5-6 magnitudes, whereas the greater D_r values for the M7 magnitude may be related to the M7 ground motions features, whose frequency content seems to be compatible with most soil profiles. It is clear from the figure that for the C site class, and particularly the M5 magnitude, the D_r ratio is distributed differently for lower and higher $\tilde{a}_0$ values, and that it varies significantly around the mean trend curve (fit curve). This depends on how the characteristics of the soil profile allow the site or SSI impacts to predominate through the position of the soil's TF curve about either the site or site + SSI TF curves (Fig. 11). According to these curves, SSI effects are significant and, therefore, more detrimental to the structural response than SE ones for the D class and M5 magnitudes, whereas the two combined effects decrease for the M6-7 magnitudes, where the D_r ratio remains close to unity and replicates results from TF curves due to nonlinear effects and offset with the superstructure features.

8.3.3 Building with s = 2

The building with s = 2 represents a range of averagely flexible buildings and one would not expect the occurrence of SSI effects due to the weakness of the $\tilde{a}_0$ ratio compared to the other buildings.

Indeed, SSIE and SE are similar for A-B classes and M5-6 magnitudes, and the lower values of the D_r ratio are produced by a de-amplification of the site response caused by the M5-6 ground motions, which are far from fundamental features of the superstructure with a relatively long resonant period (Fig. 16). For the M7 magnitude, the seismic input that includes ground motions rich in long-period components amplifies the structural response of the more flexible SFS systems and so, the site + SSI effects compared to SE. For the D class and M5 magnitude, SSIE have no influence when they are seen alone, whereas when combined with SE, it produces a more significant response than the SE one (Fig. 12), and results in consistent D_r ratio values. Nevertheless, for the M6-7 magnitudes, the site + SSI response is reduced to the same extent as for the SE one, for the same reasons as for the s = 1.5 building.

8.4 Average Maximal Base Shear Ratio

Seismic BS represents the key parameter in conventional seismic design. In the FB condition and for simple oscillator (1-DOF) systems, it may simply be obtained by multiplying the global structural stiffness by the roof displacement. Nevertheless, for the flexible-base one, it is calculated using the equivalent stiffness of the SFS system, including static soil stiffness along all modes considered. Equivalent stiffness refers to the stiffness of a FB 1-DOF replacement oscillator having the properties of the associated flexible-base system. According to Veletsos and Meek [65], the replacement oscillator would deform with a stiffness that includes a portion of the soil stiffness contribution in the equivalent system. The familiar summation rule allows estimating the equivalent stiffness as follows:

$$\frac{1}{\tilde{k}} = \frac{1}{k} + \frac{1}{k_x} + \frac{h^2}{k_\varphi} \tag{28}$$

where $\tilde{k}$ is the equivalent stiffness of the replacement oscillator. The displacements relate, respectively, to the fixed and flexible base conditions, both including SE. Further, considering the BS ratio, B_r (Eq. 29), results in values that represent displacement ratios affected by a coefficient denoting the stiffness ratio of the FB and SFS systems both with SE, whereas in all cases, this ratio is less than unity since, to some extent, the SFS stiffness is less than the FB one. Because the BS result shows the same pattern as the displacement ratio results, only findings related to the s = 1 building types are addressed and discussed. Results relating to the other buildings are provided in the appendix below.

$$B_r = \frac{b_{SSI+SE}}{b_{SE}} \tag{29}$$

In Eq. 29, b_{SSI} and b_{SE} are the mean maximal seismic BS in the SFS and site conditions, respectively.

8.4.1 Building with s = 1

Figure 17 displays the analysis's findings in the form of a seismic BS ratio along with the best fit produced by a linear regression versus $\tilde{a}_0$ ratio. Each point on the related curves reflects the BS ratio between the conditions of the SFS + SE and the FB + SE, corresponding, respectively, to a FB

system on a site class and a flexible base system that takes into account the presence of the same site class.

The values of the BS ratio associated with M5–6 magnitudes for A and B classes indicate an absence of site and SSI effects, because of soil hardness with lower $\tilde{a}_0$ ratios, having pushed the FB + SE condition to produce less visible BS. The influence of ground motions with rich long-period pulses that are somewhat far away from SFS system periods is explained by the M7 magnitude's little trend for the BS ratio to decrease. For systems whose soil properties match those of the seismic input, a partial predominance of SSIE is shown in the B class with M5 magnitude. The latter is distinguished by short-period components that are consistent with the building type's attributes. The SFS response was moderately dominant in the case of B class with M6 magnitude due to correlation with the features of the seismic input, In contrast, the curves for the M7 magnitude show disagreement with the seismic input features because of an offset with the systems that were analyzed. This conclusion can be reached by observing the equivalence between the two effects through the associated TF curves related to M6-7 magnitudes.

Due to the significance of the $\tilde{a}_0$ ratio, SSI effects are dominant for the C class and are predicted to have an impact on building types for all magnitudes. However, results confirmed by the related TF curves (Fig. 10) let us draw the conclusion that the SFS condition governs the seismic response in terms of BS for this low-rise building, which also supports findings made by Çelebi et al. [17] and Khosravikia et al. [13]. The same trend would be expected for the D class due to the important $\tilde{a}_0$ ratios, but equivalence between the two effects is found to be lower due to a more reduced SSI response. Furthermore, a significant attenuation of the response is perceived for the M6-7 magnitudes due to a clear contribution of the damping effect, indicating the nonlinear behavior of soil materials.

8.5 Statistical Features of the Average Maximal Base Shear Ratio

The fitted linear curves of Fig. 18 resulting from a linear regression may represent the simpler representation of the structural response within a flexible-base condition inside a regulatory framework, considering or disregarding the SE influence. However, the linear relationship of the B_r model may not be quantitatively reliable unless certain conditions are met. For this purpose, the expected value of the error terms (mean residuals) should be zero and have a scatter without a particular shape, i.e., their variance should be the same for all values of the related parameter B_r, as well as follow a normal probability distribution law. In this regard, observing Figs. 18 and 19 enables us to conclude that the linear model may be adopted as a good indicator of the impact of SE on the flexible-base building response within the EC-8 site classification scheme, especially for the A, B, C, and D classes and M7 magnitude, where a reasonably good distribution of the error terms is observed.

On the other hand, the distribution of the error terms for the B class and M5 magnitude appears to be skewed to the left, and the linear model can only be effective at lower values of the $\tilde{a}_0$ ratio due to the linear progression of the error terms variance beyond $\tilde{a}_0 = 0.13$ (Fig. 18). Nevertheless, the Br's residual distribution frequencies are skewed, forcing the model to be retained only for lower values of the $\tilde{a}_0$ ratio, even though the variance trend is not as dispersed as for the M5 magnitude (Fig. 19). According to the associated curve (Fig. 18) and the D class with M6 magnitude, it is obvious that the error term distribution shifts and the variance tends to decrease toward the greater values of $\tilde{a}_0$, allowing one to conclude that the linear model is reliable only for the higher values of the $\tilde{a}_0$ ratio.

9 Conclusions

Structural design is still conducted with the assumption of a fixed base, as per various seismic code provisions. In many cases, this assumption results in conservative outcomes from the perspective of structural dimensioning. SE, on the other hand, are taken into account on a flat-rate basis via the code-provisions site factor, which does not account for the ground shaking level or structure's dynamic properties. Additionally, SSI studies are frequently regarded by the engineering community as specific analyzes that are expected to occur in particular geological conditions, regardless of the earthquake magnitude. The paper examined the dynamic response of coupled SFS systems associated with SE including the influence of seismic magnitude, within the regulatory framework of EC-8 and ASCE7-16 provisions. The key findings indicate that, depending on the earthquake intensity, the type of building connected to the local geology generates a dynamic structural response that is controlled by either site or SSI effects. In light of the study's results related mainly to the D_r and B_r ratios, the following conclusions may be drawn:

- The combination of the site and SSI effects produces a structural response that is overall governed by soil features in terms of frequency and by either site or SSI effects in terms of amplitude.
- Except for the $s = 1.5$ building and M7 magnitude, where the earthquake features appear to have strongly reacted with the SFS systems, there is no significant impact of either SSI or site effects within the A class, which can be assimilated to the fixed-base condition. The B site class is often regarded as being markedly

close to the A site class, where site or SSI effects are not expected. This may be accepted for all building types and M5 magnitude, while a slight dominance of SSIE is observed in the other cases, but this depends on the earthquake features related to the seismic magnitude.

- The C site class represents the more advantageous scenario in which SSIE are expected to be apparent for low-rise buildings (s = 1). The results show that SSIE govern the structural response, with a developing trend toward the less consistent side of soil profiles. For the D class, they result in a more attenuated response if the SE are disregarded. However, the offset with the building features forced the combined response to be controlled more by SE.
- The SSIE somewhat raised the overall structural reaction for structures with s = 1.5, particularly for the M6 magnitude in the C class and, more specifically, for the D class and M5 magnitude, leading to the conclusion that the SSIE regulates the structural response.
- The relevant findings and fitted linear curves from a linear regression for the two ratios were also displayed in light of the connected statistical aspects. The linear models work well as indicators to demonstrate the impact of the flexible-base condition, with or without SE. However, the models' use depends on the kind of site soil and the seismic input properties when they are observed from a quantitative point of view.
- The investigations allowed for the identification of changes in the combined structural response resulting from the flexible base condition as compared to the FB one, where both conditions contain SE. The analysis's results also made it easier to understand how the seismic environment affected these changes.

Appendix

Figs. 20, 21, 22, 23, 24, 25

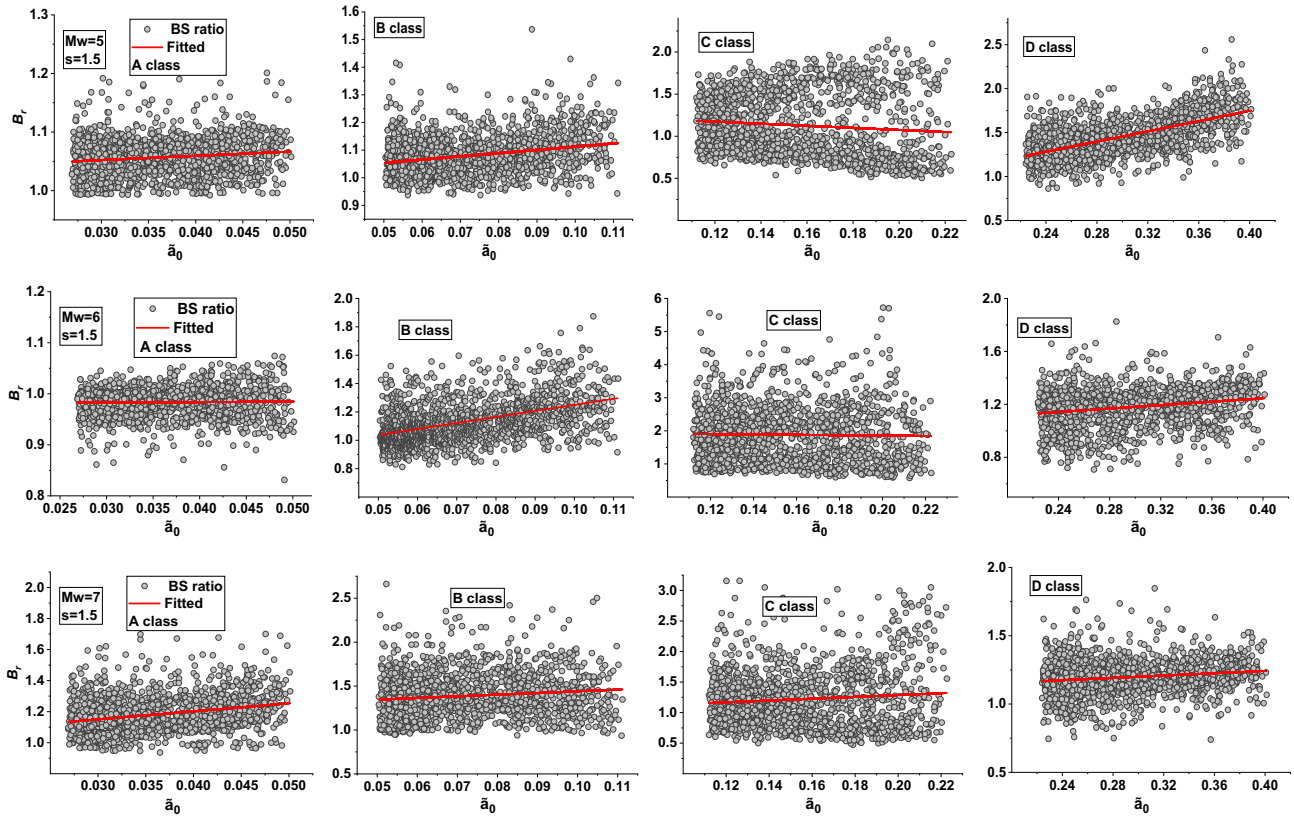

Fig. 20 Base shear ratio versus soil-to-structure stiffness ratio with the best fit for the s = 1.5 building with M = 5–6-7

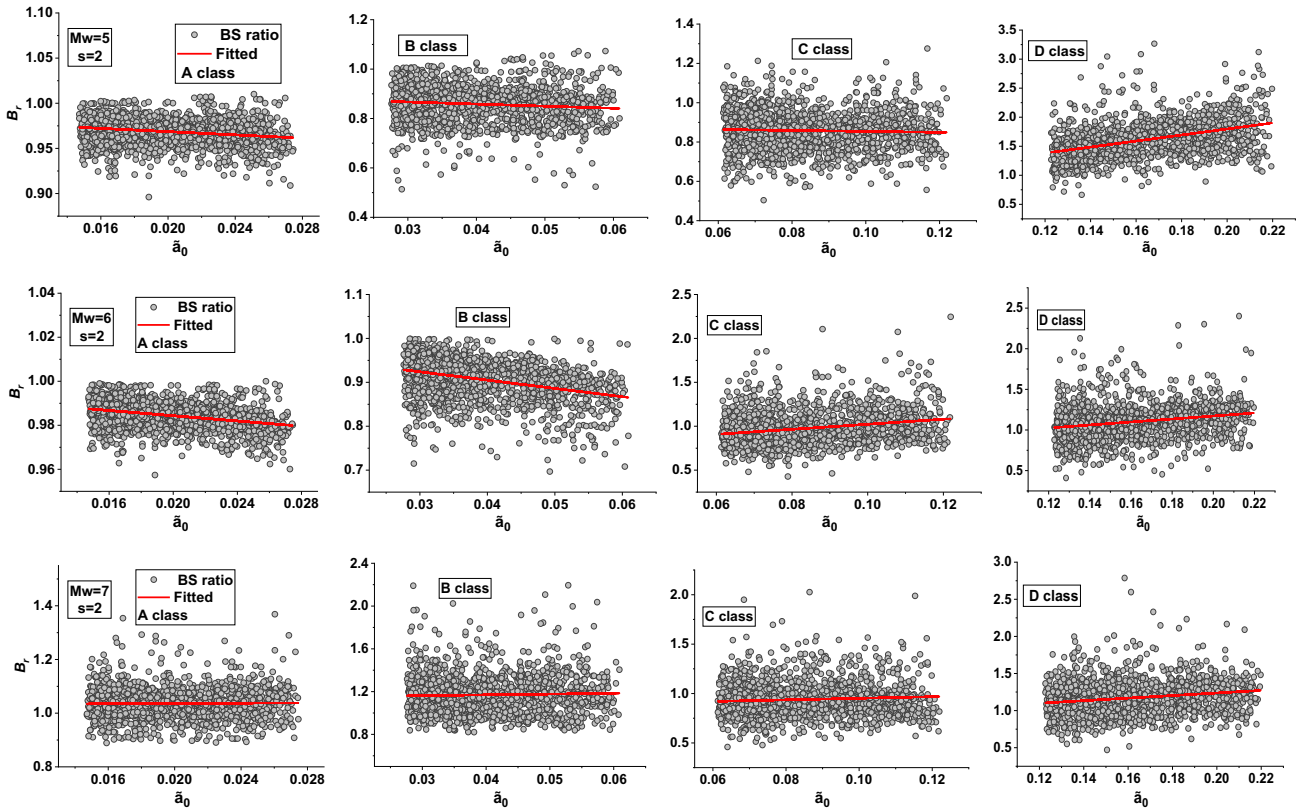

Fig. 21 Base shear ratio versus soil-to-structure stiffness ratio with the best fit for the s = 2 building with M = 5–6-7

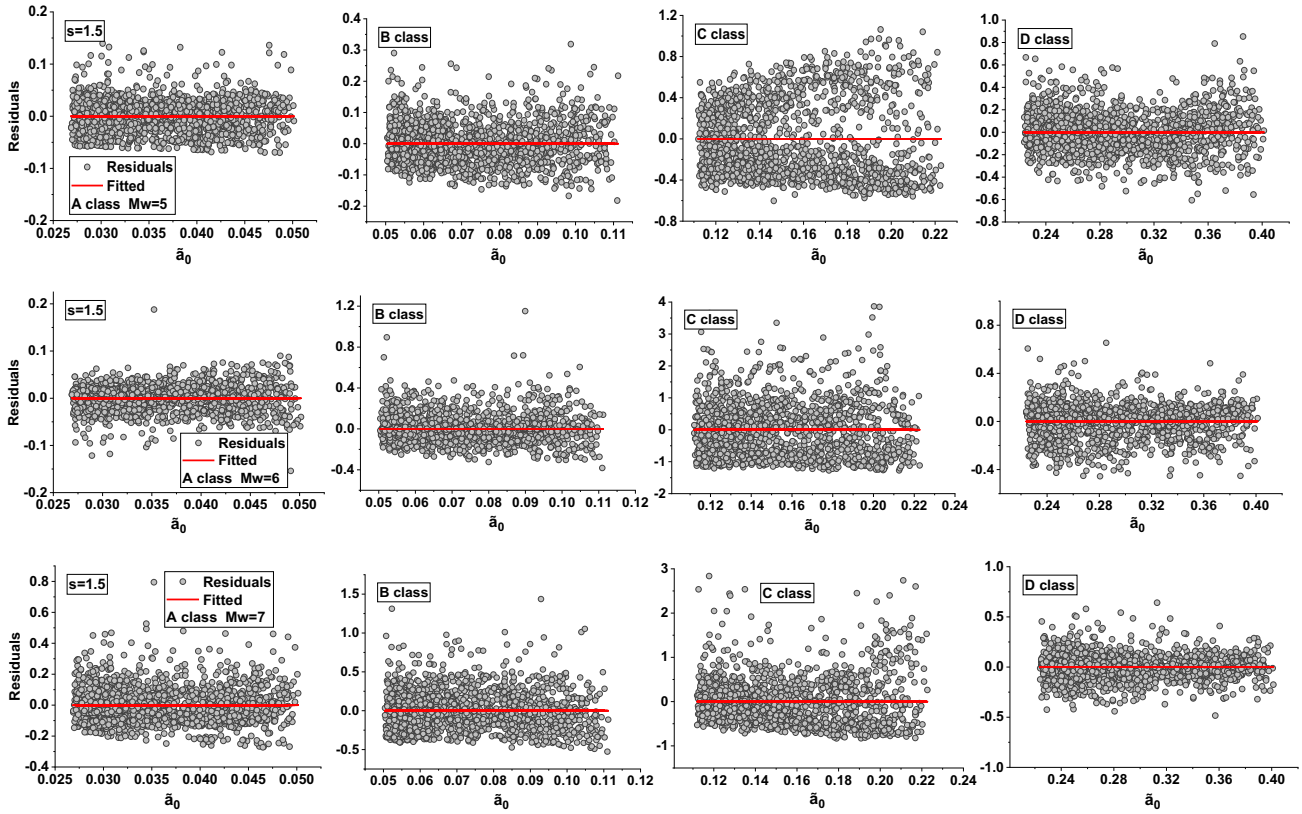

Fig. 22 Residuals versus $\tilde{a}_0$ ratio relative to the corresponding linear regression fit curve of the B_r ratio results related to the s = 1.5 building for all magnitudes and all site classes

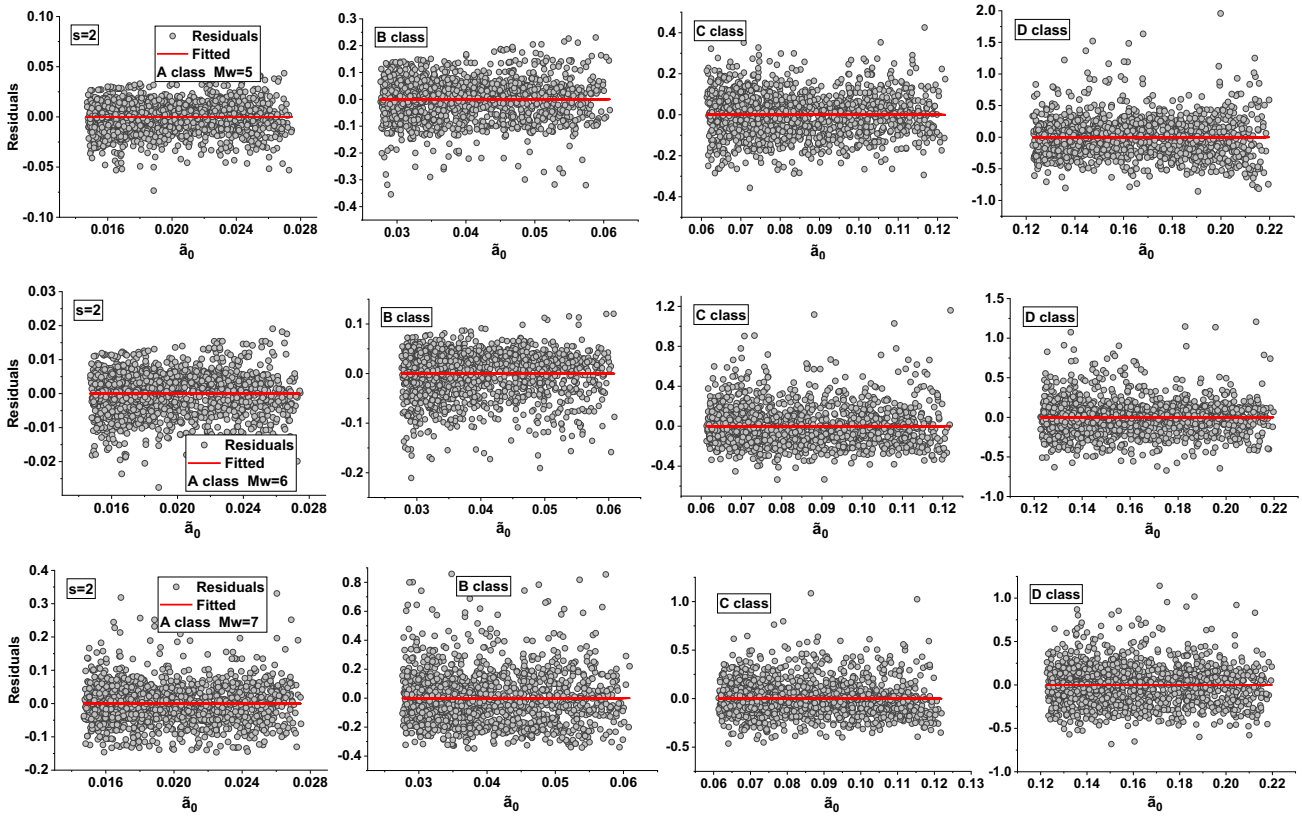

Fig. 23 Residuals versus $\tilde{a}_0$ ratio relative to the corresponding linear regression fit curve of the B_r ratio results related to the $s = 2$ building for all magnitudes and all site classes

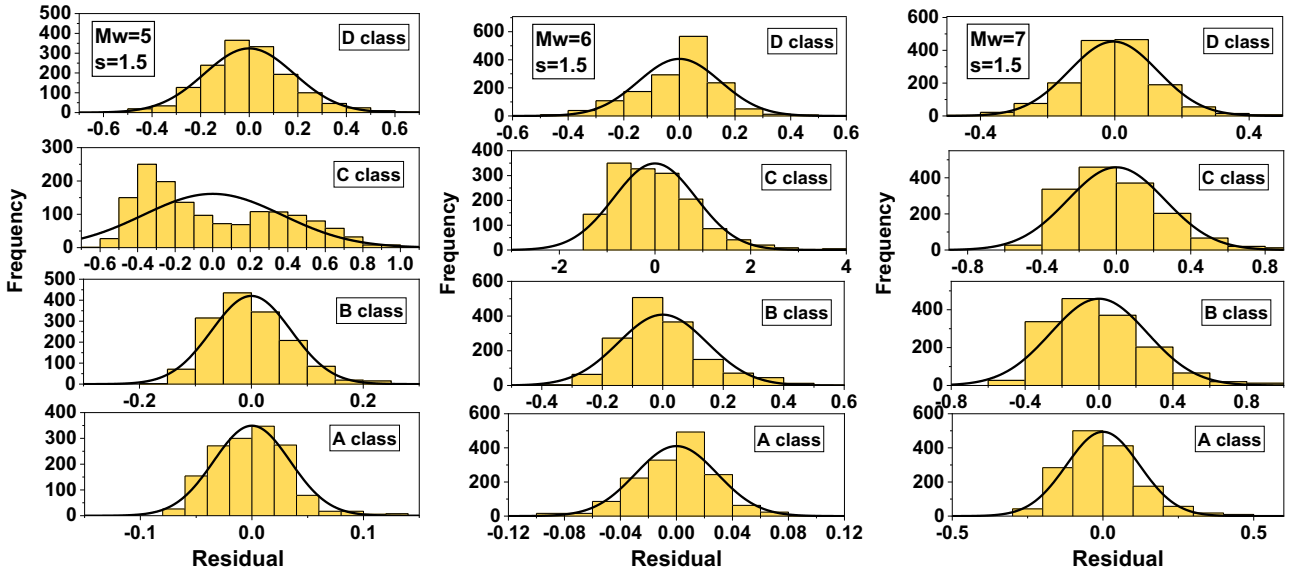

Fig. 24 Distribution of the residuals of the B_r's linear regression model along with the distribution curve of the $s = 1.5$ building, for all magnitudes and all site classes

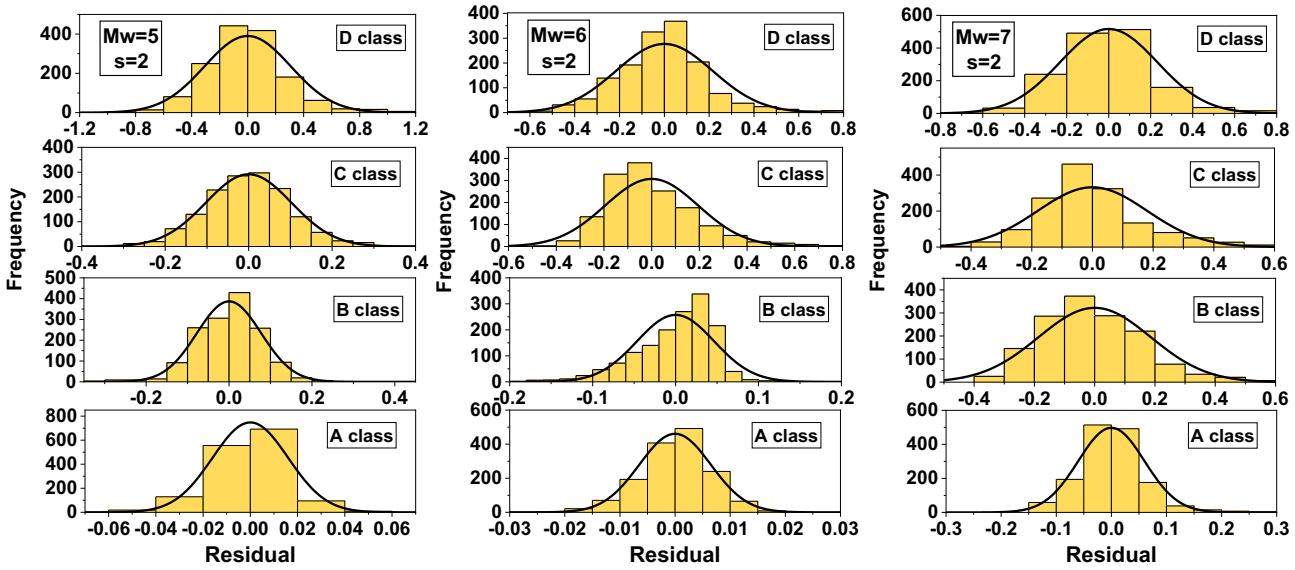

Fig. 25 Distribution of the residuals of the B_r's linear regression model along with the distribution curve of the $s = 2$ building, for all magnitudes and all site classes

Author contributions All authors contributed to the study conception and design. Material preparation, and analysis were performed by [Mohamed Beneldjouzi], [Mohamed Hadid], [Nasser Laouami] and [Mustapha Remki]. The first draft of the manuscript was written by [Mohamed Beneldjouzi] and all authors commented on previous versions of the manuscript. All authors read and approved the final manuscript.

Funding The authors have no relevant financial or non-financial interests to disclose.

Data availability The authors declare that all data and supporting information for the study's findings are contained in the paper itself.

Declarations

Conflict of interest The authors declare that no funds, grants, or other support was received during the preparation of this manuscript.

References

1. Glass CE (1989) A focus on the 1985 September Michoacan earthquakes (1985). Int J Min Geol Eng 7:9–15. https://doi.org/10.1007/BF01552835
2. Mayoral JM, Asimaki D, Tepalcapa S, Wood C, Roman-de la Sancha A, Hutchinson FTK, Montalva G (2019) Site effects in Mexico City basin: past and present. Soil Dyn Earthq Eng 121:369–382
3. Mavroeidis GP, Dong G, Papageorgiou AS (2004) Nearfault ground motions and the response of elastic and inelastic single-degree-of-freedom (SDOF) systems. Earthq Eng Struct Dyn 33:1023–1049
4. Mavroeidis GP, Papageorgiou AS (2010) Effect of fault rupture characteristics on near-fault strong ground motions. Bull Seismol Soc Am 100:37–58
5. He S, Chen T, Vennes I, He X, Song D, Chen J, Mitri H (2020) Dynamic modelling of seismic wave propagation due to a remote seismic source: a case study. Rock Mech Rock Eng 53:5177–5201
6. Aki K (1993) Local site effects on weak and strong ground motion. In: Lund F (ed) New horizons in strong motion: seismic studies and engineering practice. Tectonophysics, Netherlands, pp 1–3
7. Cadet H, Bard PY, Rodriguez-Marek A (2012) Site effect assessment using KiK-net data: part 1. A simple correction procedure for surface/downhole spectral ratios. Bullet Earthquake Eng 10(2):421–448
8. Wong HL, Luco JE (1986) Dynamic interaction between rigid foundations in a layered half space. Earthquake Eng Struct Dynam 5(3):149–158. https://doi.org/10.1016/0267-7261(86)90018-7
9. Stewart JP, Seed RB, Fenves GL (1999) Seismic soil-structure interaction in buildings I: analytical aspects. J Geotech Geo Environ Eng 125:26–37
10. Aviles J, Pérez-Rocha LE (1998) Site effects and soil-structure interaction in the valley of Mexico. Soil Dyn Earthq Eng 17:29–39
11. Fatahi B, Tabatabaiefar SHR, Samali B (2014) Soil-structure interaction vs Site effect for seismic design of tall buildings on soft soil. Geomech Eng 6(3):293–320
12. Sayyadpour H, Behnamfar F, El Naggar MH (2016) The near-field method: a modified equivalent linear method for dynamic soil–structure interaction analysis. Part II: verification and example application. Bull Earthq Eng 14:2385–2404. https://doi.org/10.1007/s10518-016-9871-1
13. Khosravikia F, Mahsuli M, Ghannad MA (2018) The effect of soil–structure interaction on the seismic risk to buildings. Bull Earthq Eng 16:3653–3673. https://doi.org/10.1007/s10518-018-0314-z
14. Brunelli A, de Silva F, Cattari S (2022) Site effects and soil-foundation-structure interaction: derivation of fragility curves and comparison with Codes-conforming approaches for a masonry school. Soil Dyn Earthq Eng. https://doi.org/10.1016/j.soildyn.2021.107125
15. Dutta SCRR (2002) A critical review on idealization and modeling for interaction among soil–foundation–structure system.

Comput Struct 80(20–21):1579–1594. https://doi.org/10.1016/S0045-7949(02)00115-3
16. Çelebi E, Göktepe F, Karahan N (2012) Non-linear finite element analysis for prediction of seismic response of buildings considering soil-structure interaction. Nat Hazard 12(11):3495–3505
17. Deoda VR, Adhikary S (2020) Use of conditional mean spectra for seismic evaluation of RC building considering soil effects. Int J Civil Eng. https://doi.org/10.1007/s40999-020-00536-1
18. Eurocode 8 (2004) Design of structures for earthquake resistance-Part I: general rules, seismic actions and rules for buildings. European Committee for Standardization, Brussels, Belgium
19. American Society of Civil Engineers (2016) Minimum design loads for buildings and other structures. ASCE standard, ASCE/SEI 7–16 ASCE Virginia. ISBN 978–0–7844–7996–4
20. Ayadi A, Ousadou F, Roumane K, Harbi A, Maouche S, Bezzeghoud M, Meghraoui M (2021) An update of Algerian's seismic catalog from historical seismicity, archeoseismological, and paleoseismological studies. Arab J Geosci 14:1025. https://doi.org/10.1007/s12517-021-07348-0
21. Bouhadad Y, Laouami N (2002) Earthquake Hazard assessment in the Oran region (northwest Algeria). Nat Hazards 26:227–243
22. Laouami N, Slimani A (2013) Earthquake induced site effect in the algiers-boumerdes region: relation between spectral ratios higher peaks and observed damage during the may 21st Mw 6.8 boumerdes earthquake (Algeria). Pure Appl Geophys 170:1785–1801. https://doi.org/10.1007/s00024-012-0612-3
23. Ayadi K, Semmane F, Yelles-Chaouch AK (2016) Site-effects investigation in the City of Chlef (Formerly El-Asnam), Algeria, using earthquake and ambient vibration data. Bull Seismol Soc Am 106(5):2185–2196
24. Beneldjouzi M, Laouami N, Slimani A (2017) Numerical and random simulation procedure for a preliminary local site characterization and site factor assessing. Earthquake Struct 13(1):79–87
25. Chabane S, Bezzeghoud M, Fontiela J, Machane D, Oubaiche E, Bensalem R (2019) Site effects in Algiers area, Algeria. Chapter in book: Workshop em Ciências da Terra e do Espaço. Publisher: Universidade de Évora
26. RPA99 (2003) Règles Parasismiques Algériennes. D.T.R. –B.C. 2.48. Centre National de Recherche appliquée en génie parasismique (CGS), Rue Kaddour Rahim, BP 252, Hussein Dey, Alger, Algerie, Ministère de l'habitat. Imprimé par l'Office Nationale des Publications Universitaires (OPU). ISBN 9961–923–13–8
27. Beneldjouzi M, Laouami N (2015) A stochastic based approach for a new site classification method: application to the Algerian seismic code. Earthq Eng Eng Vib 14:663–681. https://doi.org/10.1007/s11803-015-0052-z
28. Borcherdt RD (1994) Estimates of site-dependent response spectra for design (methodology and justification). Earthq Spectra 10:617–653
29. Zhao JX, Irikura K, Zhang J, Fukushima Y, Somerville PG, Asano A, Saiki T, Okada H, Takahashi T (2004) Site classification for strong strong-motion stations in Japan using H/V response spectral ratio. Proceeding of the 13th World Conference on Earthquake Engineering, Vancouver, B.C., Canada
30. Fukushima Y, Bonilla LF, Scotti O, Douglas J (2007) Site Classification Using Horizontal-to-vertical response spectral ratios and its impact when deriving empirical ground motion prediction equations. J Earthquake Eng 11(5):712–724
31. Ghasemi H, Zare M, Fukushima Y, Sinaeian F (2009) Applying empirical method in site classification, using response spectral ratio (H/V): a case study on Iranian strong motion network (ISMN). Soil Dyn Earthq Eng 29:121–132
32. Boore DM, Joyner WB (1997) Site amplifications for generic rock sites. Bull Seismol Soc Am 87(2):327–341
33. Dobry R, Borcherdt RD, Crouse CB, Idriss IM, Joyner WB, Martin G, Power MS, Rinne EE, Seed RB (2000) New site coefficients and site classification system used in recent building seismic code provisions. Earthq Spectra 16:41–67
34. Choi Y, Stewart JP (2005) Nonlinear site amplification as function of 30 m shear wave velocity. Earthq Spectra 21(1):1–30
35. Veletsos AS, Prasad AM (1989) Seismic interaction of structures and soils: stochastic approach. J Struct Eng 115(4):935–956
36. Hamadache M, Peláez JA, Talbi A, Casado CL (2010) A Unified catalog of main earthquakes for northern Algeria. Seismol Res Lett 81(5):732–739. https://doi.org/10.1785/gssrl.81.5.732
37. Fenton GA, Griffiths DV (2003) Bearing-capacity prediction of spatially random c–ϕ soils. Can Geotech J 40:1. https://doi.org/10.1139/t02-086
38. Vucetic M (1994) Cyclic threshold shear strains in soils. J Geotech Eng 120(12):2208–2228
39. Seed HB, Idriss IM (1970) Soil moduli and damping factors for dynamic response analyses. Earthquake Engineering Research Center. Report N° EERC 70–10. University of California Berkley. California
40. Hardin BO, Drnevich VP (1972) Shear modulus and damping in soils: measurement and parameter effects (Terzaghi lecture). J Soil Mech Found Div 98(6):603–624
41. Lee MKW, Finn WDL (1978) DESRA-2: Dynamic effective stress response analysis of soil deposits with energy transmitting boundary including assessment of liquefaction potential (book). University of British Columbia, Department of Civil Engineering
42. Sun JI, Golesorkhi R, Seed HB (1988) Dynamic moduli and damping ratios for cohesive soils Report N° UCB/EERC-88/15. University of California, Berkeley, California, Earthquake Engineering Research Center
43. Ishibashi I, Zhang X (1993) Unified dynamic shear modulus and damping ratios of sand and clay. Soils Found 33(1):182–191
44. Darendelli MB (2001) Development of a new family of normalized modulus reduction and material damping curves. PhD Dissertation. Department of Civil, Architectural, and Environmental Engineering, University of Texas at Austin. http://hdl.handle.net/2152/10396
45. Menq FY (2003) Dynamic Properties of Sandy and Gravelly Soils. PhD Dissertation. Department of Civil, Architectural, and Environmental Engineering, University of Texas at Austin. http://hdl.handle.net/2152/779
46. Oztoprak S, Bolton MD (2013) Stiffness of sands through a laboratory test database. Géotechnique 63(1):54–70
47. Wolf JP (1985) Dynamic soil-structure interaction. Prentice-Hall Inc, Englewood Cliffs, New Jersey, p 07632
48. Hadid M, Afra A (2000) Sensitivity analysis of site effects on response spectra of pipelines. Soil Dyn Earthq Eng 20:249–260
49. Kanai K (1957) Semi-empirical formula for the seismic characteristics of the ground. Bull Earthq Res Inst 35(2):309–325
50. Tajimi HA (1960) Statistical method of determining the maximum response of a building structure during an earthquake. In: Proceedings of the second world conference on earthquake engineering, Volume 3, Science Council of Japan. Tokyo and Kyoto, Japan
51. Veletsos AS (1974) Dynamic behaviour of building-foundation systems. Earth Eng and Stru Dyn 3:121–138. https://doi.org/10.1002/eqe.4290030203
52. Pais A, Kausel E (1988) Approximate formulas for dynamic stiffness of rigid foundations. Soil Dyn Earthq Eng 7(4):213–227
53. Gazetas G (1991) Foundation vibrations. Chapter in foundation engineering handbook. 2nd ed. Van Nostrand Reinhold. pp 553–93. Springer, Boston, MA
54. Laouam N, Slimani A, Larbes S (2018) Ground motion prediction equations for Algeria and surrounding region using site

classification-based H/V spectral ratio. Bull Earthquake Eng 16:2653–2684. https://doi.org/10.1007/s10518-018-0310-3
55. Vanmarcke EH, Gasparini DA (1977) Simulated earthquake ground motions. SMiRT 4 publisher - San Francisco, USA. http://www.lib.ncsu.edu/resolver/1840.20/27894
56. Gilbert RJ (1988) Vibration des structures. Edition Eyrolles Paris, ISSN 0 3 9 9 - 4 1 9 8
57. Jennings PC, Housner GW, Tsai C (1969) Simulated earthquake motions for design purpose. Technical Report N° CaltechEERL: 1968.EERL.1968.001. https://resolver.caltech.edu/CaltechEERL:1968.EERL.1968.001
58. Shinozuka M, Deodatis G (1988) Stochastic process models for earthquake ground motion. Probab Eng Mech 3:114–123
59. Elsabee F, Morray JP (1977) Dynamic behavior of embedded foundations. Rep. No. R77–33, MIT-CE-R77–33. Dept. of Civ. Eng, MIT Cambridge Massachusetts USA
60. Kausel E (1974) Forced vibrations of circular foundations on layered media. Thesis, Dept. of Civ. Eng. MIT Massachusetts USA. http://hdl.handle.net/1721.1/13842
61. Olsen K, Day S, Bradley C (2003) Estimation of Q for long-period (> 2sec) waves in the Los Angeles basin. Bull Seismol Soc Am 93:627–638
62. Maravas A, Milonakis G, Karabalis DL (2014) Simplified discrete systems for dynamic analysis of structures on footings and piles. Soil Dyn and Earth Eng 61–62:29–39
63. FEMA P-2091 (2020) A Practical Guide to Soil-Structure Interaction. Prepared by Applied Technology Council for Federal Emergency Management Agency Washington DC.
64. Tabatabaiefar HR, Massumi A (2010) A simplified method to determine seismic responses of reinforced concrete moment resisting building frames under influence of soil–structure interaction. Soil Dyn Earthq Eng 30(11):1259–1267
65. Veletsos AS, Meek JW (1974) Dynamic behavior of building-foundation systems. Earthquake Eng Struct Dyn 3:121–138